Energy Efficiency Optimization of FBMC/OQAM-based Massive MIMO Systems Subject to Electromagnetic Exposure Constraints

Sudhakar Rai, Prem Singh, *Member, IEEE*, Ekant Sharma, *Senior Member, IEEE*, Aditya K. Jagannatham, *Senior Member, IEEE*, and Lajos Hanzo, *Life Fellow, IEEE*

***Abstract*—The performance of offset-quadrature-amplitude-modulated filter bank multi-carrier (FBMC/OQAM) waveform based on massive multiple-input multiple-output (MIMO) systems is investigated considering not only the transceiver's classic metrics, but also the health concerns associated with exposure to electromagnetic fields (EMF). Closed-form expressions are obtained for the lower-bounds on the uplink spectral efficiency (SE) for FBMC/OQAM-based Massive MIMO systems with both the maximum ratio combiner (MRC) and zero-forcing (ZF) receivers, in the face of realistic imperfect channel state information (CSI). Subsequently, by employing our closed-form SE expressions, a framework is developed for maximizing the global energy efficiency (GEE) of the proposed FBMC/OQAM-based system subject to both power and EMF exposure constraints. A nested quadratic-transform (NQT)-based approach is proposed next for maximizing the non-convex GEE objective by first approximating it as a concave-convex function and then by applying the quadratic transform. Subsequently, a low-complexity iterative algorithm is developed that sequentially applies the Lagrangian dual transform, quadratic transform and Dinkelbach's transform to obtain a closed-form solution of the GEE optimization problem formulated. Our simulation results verify the analytical SE expressions and also demonstrate the improved GEE of the proposed FBMC-based massive MIMO systems subject to the EMF exposure limits.**

***Index Terms*—multi-carrier modulation, FBMC/OQAM, intrinsic interference, EMF exposure, massive MIMO, energy efficiency, nested quadratic-transform, Lagrangian dual transform.**

I. Introduction

Offset-quadrature-amplitude-modulation-based filter bank multicarrier (FBMC/OQAM) signaling is one of the candidate waveforms for next-generation wireless systems [1]. The main difference between FBMC/OQAM and the popular orthogonal frequency division multiplexing (OFDM) waveform lies in the choice of the synthesis and analysis filters used at the transmitter and receiver, respectively [2]. Contrary to OFDM, FBMC/OQAM employs bespoke frequency-time (FT) filters for subcarrier shaping, which make it resilient to both time and frequency dispersions [3]. As a result, FBMC/OQAM results in significantly lower out-of-band (OOB) leakage in comparison to OFDM that shapes each of its subcarriers using a rectangular time-domain pulse having a sinc-shaped spectrum [4]. Moreover, FBMC/OQAM signals do not require guard interval, i.e., cyclic prefix, which improves their spectral efficiency (SE) [5]. Due to the above-mentioned properties, FBMC/OQAM waveform has been extensively studied in conjunction with single-input single-output (SISO) [5], [6], multiple-input multiple-output (MIMO) [7]–[12], massive MIMO [13]–[21] and millimeter wave [22] technologies.

The authors of [3] demonstrated the superiority of the FBMC waveform in comparison to the OFDM waveform using both simulations and real-world test-bed results. Since FBMC/OQAM obeys only real-domain orthogonality, it is vulnerable to interference in the imaginary domain, which termed intrinsic interference. This renders channel estimation and equalization of FBMC/OQAM challenging. To address this, the interference approximation method (IAM) has received extensive research attention toward the estimation of the channel in FBMC/OQAM systems [7], [8]. The authors of [23] proposed a novel approach for intrinsic interference cancellation by enabling the transmission of QAM symbols in an FBMC/OQAM system using the repeated frame structure. Similarly, the authors of [6] proposed low-complexity symbol reconstruction techniques based on the interference avoidance method relying on dual pilot symbols.

Many solutions have been proposed in the literature to mitigate the virtual interference in an FBMC waveform in order for it to be seamlessly coupled with MIMO technology in both uplink and downlink transmissions. These studies mainly focused on i) MIMO-FBMC/OQAM systems [9]–[12]; and ii) FBMC/QAM systems [24]. The authors of [11] proposed an FFT-FBMC system that performs the IDFT and DFT operations at the transmitter and receiver, respectively, to render the FBMC compatible with MIMO technology. Nissel *et al.,* [9], proposed a computationally efficient scheme for mitigating the intrinsic interference arising in a MIMO-FBMC/OQAM system by spreading symbols in the time domain via Hadamard precoding matrix. Recently, the authors of [12], designed MIMO schemes for FBMC/OQAM systems by designing

Lajos Hanzo would like to acknowledge the financial support of the Engineering and Physical Sciences Research Council projects EP/W016605/1, EP/X01228X/1, EP/Y026721/1, EP/W032635/1 and EP/X04047X/1 as well as of the European Research Council's Advanced Fellow Grant QuantCom (Grant No. 789028). Prem Singh would like to acknowledge the financial support under the project "CRG/2022/005251" from the Science and Engineering Research Board (SERB). Ekant Sharma would like to acknowledge the financial support under the project "ITB-1983-ECD" from IIITB COMET Foundation.

Sudhakar Rai and Aditya K. Jagannatham are with the Department of Electrical Engineering, Indian Institute of Technology Kanpur, Kanpur 208016, India (e-mail: sudhrai@iitk.ac.in; adityaj@iitk.ac.in).

Prem Singh is with the ECE Department, IIIT Bangalore, Bengaluru 560100, India (e-mail: prem.singh@iiitb.ac.in).

Ekant Sharma is with the Department of Electronics and Communication Engineering, Indian Institute of Technology Roorkee, Roorkee, Uttarakhand 247667, India (e-mail: ekant@ece.iitr.ac.in).

Lajos Hanzo is with the School of Electronics and Computer Science, University of Southampton, Southampton SO17 1BJ, U.K. (email:lh@ecs.soton.ac.uk).

the singular value decomposition (SVD)-and subband-based precoding schemes by relying on repeated blocks with the reverse arrangement of symbols at the transmitter. In addition, another variant of FBMC modulation, FBMC/QAM has also gained research attention for its ability to mitigate inherent interference and support MIMO transmission [24]. The FBMC/QAM system comprises two prototype filters, one for even-numbered and the other for odd-numbered subcarrier symbols. The intelligent combinations of these filters satisfies complex-domain orthogonality and, therefore, cancels the intrinsic interference, which allows for the transmission of complex-valued symbols [24].

The rapid technological advances in the field of wireless networks along with the evolution of consumer electronics technology have given rise to new applications, such as Artificial Intelligence (AI), Extended Reality, Internet of Things (IoT) etc., which have lead to the proliferation of wireless devices [25], [26]. These devices emit electromagnetic (EM) radiation that poses a potential health risk to human users. Hence, such devices must adhere to tight regulations to limit the EM exposure level of users [27]. Needless to say, exposition to the EM field during the operation of wireless devices is a critical issue for future wireless networks and has to be investigated to address the safety concerns of users [28].

To this end, the specific absorption rate (SAR), which expresses the absorbed power per unit mass of human tissues in terms of the unit W/kg, has become a standard metric for determining the EM exposure level in a frequency range of 100 KHz - 10 MHz [29]. Various studies have been conducted to assess the SAR to protect against adverse health effects. The adverse effect of a high SAR value can be seen as a rise in the temperature of the body part exposed. Experimental investigations verify that exposure to intense EM field, which results in 1 degree Celsius rise in body temperature, leads to detrimental health impacts. The factors that influence the evaluation of the SAR value include operating frequency, antenna design (type/size/number), dielectric properties (homogeneous/heterogeneous) of body parts (Head/Torso/Wrist/ankles), body-worn device vs handheld device and use case (Voice/Data/Machine-type communication), etc [30]. The acceptable SAR limits have been widely standardized by regulatory bodies throughout the world, such as the Federal Communications Commission (FCC) in the United States (US) and the International Commission on Non-Ionizing Radiation Protection (ICNIRP) in other parts of the world [31]. The focus of this treatise is to investigate the spectral and energy efficiency of FBMC-based massive MIMO systems with a special emphasis on meeting the SAR constraints.

A. Review of existing works

The amalgamation of massive MIMO technology with the FBMC waveform was first investigated in [13], which numerically showed that multipath distortion can be avoided by exploiting the self-equalization property of massive MIMO-FBMC systems without the requirement of a flat fading channel at the individual sub-carrier level. Subsequently, Rottenberg *et al.,* in [14] validated the characterized massive MIMO-FBMC systems in their theoretical analysis. The authors of [15] derived an analytical expression for the asymptotic signal-to-interference-plus-noise-ratio (SINR) and demonstrated that a single tap equalizer is unable to completely eliminate the channel-induced dispersion in massive MIMO-FBMC systems. Aminjavaheri *et al*. designed a novel prototype filter in [16], to mitigate the residual inter-symbol interference (ISI) in FBMC-aided massive MIMO systems. To further advance, the authors of [17] explored the performance of a two-stage equalizer designed for massive MIMO-FBMC systems employing realistic imperfect channel state information (CSI). The authors of paper [18] exploit Jensen's inequality to derive the closed-form expressions for the uplink sum-rates of massive MIMO-FBMC systems. The authors of [20] designed a sophisticated FBMC receiver for a multi-user (MU)-massive MIMO system considering different channel impairments, and demonstrated remarkable robustness against time/frequency offsets, which is in stark contrast to its OFDM counterpart. More recently, QI *et al.* [21] proposed a multi-stage equalization technique for the design of a multi-tap equalizer for FBMC/OQAM-based massive MIMO systems communicating over highly-frequency selective channels. The contributions surveyed above show that FBMC is well-suited for massive MIMO-aided next-generation wireless systems.

Due to the recent exponential growth of wireless devices and applications, it is now necessary to build energy-efficient resource allocation algorithms for wireless networks. Consequently, it is essential to investigate the energy efficiency (EE) of the FBMC-based massive MIMO systems. The authors in [32] investigated the EE of cognitive radio-inspired FBMC networks. This work, however, did not consider the massive MIMO-based design. Recently, the mitigation of EM exposure has received significant attention in the design and analysis of cellular systems [33]–[40]. In particular, research in this field is classified into two categories: optimization of system performance subject to the stringent regulatory guidelines to limit the exposure [30], [33]–[35], [37], [39], [41] and minimizing the total EM exposure, while maintaining the system performance required [35], [36], [38], [40], [42]. The aim is to avoid the health risks arising due to radio frequency (RF) radiation from cellular networks, which can be accomplished by designing a cellular network in compliance with EMF constraints [39], [40]. The authors of [33] proposed an EE maximization technique for the uplink MU-MIMO system subject to both power and SAR constraints per user. The authors of [34] have studied the trade-off between SE and EE in the uplink of a MU-MIMO system subject to specific SAR constraints. The authors of [35] formulated an optimization framework for minimizing the EMF exposure subject to specific quality of service (QoS) constraints for tethered unmanned aerial vehicles (TUAVs). The authors of [36] have investigated a machine learning-based user clustering technique and proposed an EMF-aware power allocation strategy for power domain non-orthogonal multiple access (PD-NOMA) systems. More recently, Jiang *et al.*, in [37] developed an architecture constituted by a reconfigurable intelligent surface (RIS) and a dynamic metasurface antenna-assisted MU-MIMO system operating under SAR constraints. Héliot and Brown [38] designed an MU-MIMO OFDM system that minimizes the EM exposure of the users carrying wireless

devices equipped with multiple antennas.

Our contributions are contrasted at a glance to the literature in Table I. Observe that only a few treatises have investigated the SE and EE of massive MIMO-FBMC systems analytically [18], [32]. The authors of [18] derived analytical SE bounds and evaluated the performance for an asymptotically large number of base station (BS) antennas, an assumption that does not hold in practice. The existing literature on FBMC-based massive MIMO systems has not harnessed the use-and-then-forget (UatF) procedure to develop SE bounds that are valid for any number of BS antennas [43], [44, Theorem 4.4]. Furthermore, work in [32] is the only available treatise that investigated the EE of FBMC systems and there is no existing work that has investigated the EE of FBMC-based massive MIMO systems. In addition, the optimization of FBMC waveform aided massive-MIMO systems under EM exposure constraints has not been studied in the existing literature. In view of the above knowledge-gaps in the existing literature, this treatise aims for designing, analyzing and optimizing the SE and EE of EMF-aware massive MIMO-FBMC systems. In this context, the key contributions of this treatise are listed below.

1) Exploiting the UatF bounding technique, closed-form lower-bounds are derived on the uplink sum-rate for the FBMC-based massive MIMO system considering both the maximum ratio combiner (MRC) and the zero-forcing (ZF) receivers relying on realistic imperfect CSI.
2) Next, the global energy efficiency (GEE) of the considered FBMC-based massive MIMO system is maximized using the closed-form sum-rate expressions derived, subject to both user power and SAR constraints, with the latter being invoked to prevent the harmful effect of EM radiation. A nested quadratic-transform (NQT) technique is developed to solve the above SAR-restricted GEE optimization problem for FBMC-based massive MIMO systems.
3) Subsequently, a low-complexity Lagrangian dual-transform (LDT)-based iterative algorithm is proposed for solving the above optimization problem, which is seen to yield a closed-form solution. The computational complexities of both the NQT and LDT-based optimization techniques are explicitly determined, which reveals that the complexity of the latter increases only linearly with the number of users, rendering it ideally suited for practical systems.
4) Finally, our simulation results verify the accuracy of the closed-form SE expressions derived and also demonstrate that the proposed optimal power allocation (OPA) yields substantially higher GEE than the equal-power allocation (EPA). Furthermore, the results also show that the optimized GEE can meet the stringent limits imposed by the ICNIRP for EMF exposure, which renders the FBMC-based massive MIMO system eminently suitable for next-generation wireless networks.

II. System Model

Consider a single-cell multi-user massive MIMO system based on the FBMC/OQAM waveform relying on M sub-carriers. There are K-single antenna users in the cell, who are simultaneously transmitting their signals to a BS equipped with an array of N antennas. Let T_s denote the duration of the QAM symbols $c^k_{m,n}$. Furthermore, let $d^k_{m,n}$ represent the real offset-QAM symbol transmitted by the kth user at the mth subcarrier index and nth symbol time index in a rectangular FT lattice. The OQAM symbols $d^k_{m,2n}$ and $d^k_{m,2n+1}$, each of duration $\frac{T_s}{2}$, are generated by splitting the real and imaginary parts of the complex-valued QAM symbols $c^k_{m,n}$ with an offset of $\frac{T_s}{2}$ as follows

$$d^k_{m,2n} = \begin{cases} \Re\big(c^k_{m,n}\big), & \text{if } m \text{ is even} \\ \Im\big(c^k_{m,n}\big), & \text{if } m \text{ is odd,} \end{cases}$$

$$d^k_{m,2n+1} = \begin{cases} \Im\big(c^k_{m,n}\big), & \text{if } m \text{ is even} \\ \Re\big(c^k_{m,n}\big), & \text{if } m \text{ is odd.} \end{cases}$$

The transmitted OQAM symbols are assumed to be temporally and spatially independent and identically distributed (i.i.d) with average power $\mathbb{E}\big[d^k_{m,n}(d^k_{m,n})^*\big] = P_k$. This also implies that $\mathbb{E}\big[c^k_{m,n}(c^k_{m,n})^*\big] = 2P_k$. The uplink channel between the BS and users is considered to be quasi-static and constant over an interval of $T = T_c B_c$, where T_c and B_c are the channel's coherence time and coherence bandwidth, respectively [48]. The coherence interval T is comprised of the training duration τ_p and data duration $\tau_d = T - \tau_p$. The next sub-section presents the data transmission model followed by the proposed channel estimation technique.

A. Data transmission model

In the data transmission period, the lth sample of the discrete-time baseband FBMC signal for the kth user is expressed as [17]

$$s_k\big[l\big] = \sum_{m=0}^{M-1} \sum_{n\in\mathbb{Z}} d^k_{m,n} \chi_{m,n}\big[l\big], \tag{1}$$

where $\chi_{m,n}\big[l\big]$ represents the FBMC signalling pulse defined as

$$\chi_{m,n}\big[l\big] = p\big[l - n\frac{M}{2}\big] e^{j\phi_{m,n}} e^{\frac{j2\pi ml}{M}}. \tag{2}$$

The variable $p\big[l\big]$ denotes the impulse response of a symmetric real-valued prototype filter of length $L_p = k_o M$ with k_o being the number of adjacent FBMC/OQAM symbols that overlap in the time domain (TD). This is in contrast to OFDM systems, wherein the symbols do not overlap in the TD due to using rectangular pulse shaping filters of length equal to the OFDM symbol duration. In an FBMC system, the length of the prototype filter is higher than that of the symbol interval, which can therefore shape each subcarrier by a prototype filter that is well localized in the FT domain. The term $\phi_{m,n} = \frac{\pi}{2}(m+n) - \pi mn$ in (2) is the phase factor introduced between adjacent subcarriers and adjacent symbols to guarantee real-domain orthogonality between the FBMC basis functions [15]. The cross-correlation between the two basis functions $\xi^{\bar{m},\bar{n}}_{m,n} = \sum_{l=-\infty}^{\infty} \chi_{m,n}\big[l\big]\chi^*_{\bar{m},\bar{n}}\big[l\big]$, defined over the FT lattice points (m,n) and $(\bar{m},\bar{n})$, can be expressed as follows:

$$\xi^{\bar{m},\bar{n}}_{m,n} = \begin{cases} 1, & \text{if } \big(m,n\big) = \big(\bar{m},\bar{n}\big) \\ \text{Imaginary}, & \text{if } \big(m,n\big) \neq \big(\bar{m},\bar{n}\big). \end{cases} \tag{3}$$

The result in (3) implies that $\Re\big\{\xi^{\bar{m},\bar{n}}_{m,n}\big\} = \delta_{m,\bar{m}}\delta_{n,\bar{n}}$, where

Table I: Contrasting our contributions to the literature.

	[5], [6]	[13]–[15]	[18]	[17], [21]	[45], [46]	[32]	[47]	**Proposed**
FBMC/OQAM	✓	✓	✓	✓	✓	✓	✓	✓
Massive-MIMO		✓	✓	✓	✓			✓
Channel Estimation			✓	✓			✓	✓
EMF Exposure								✓
Spectral Efficiency (SE)			✓	✓	✓		✓	✓
Closed-form SE				✓				✓
Energy Efficiency Optimization						✓		✓

the term $\delta_{m,\bar{m}} = 1$ for $m = \bar{m}$ and 0 for $m \neq \bar{m}$. The signal received on the rth antenna at the BS can be written as

$$y_r[l] = \sum_{k=1}^{K} \big(s_k[l] * g_{r,k}[l]\big) + \eta_r[l], \tag{4}$$

where $g_{r,k}(l)$, for $l = 1, 2, \cdots, L_h - 1$, denotes the impulse response of the L_h tap frequency selective channel between the kth user and rth antenna of the BS. The scalar $\eta_r[l]$ is the additive white Gaussian noise (AWGN) at the rth antenna which follows the $\mathcal{CN}(0, \sigma_\eta^2)$ distribution. To detect the symbol transmitted at the index $\{\bar{m}, \bar{n}\}$, $y_r[l]$ in (4) is matched with the FBMC basis function $\chi_{\bar{m},\bar{n}}$ as

$$y^r_{\bar{m},\bar{n}} = \sum_{l=-\infty}^{\infty} y_r[l]\chi^*_{\bar{m},\bar{n}}[l]. \tag{5}$$

Assuming that the maximum delay spread L_h is considerably lower than the FBMC symbol interval T_s, as is typically the case, it follows that $p\big[l - n\frac{M}{2} - \tau\big] \approx p\big[l - n\frac{M}{2}\big]$, for $\tau = 0, 1, \cdots, L_h - 1$ [5]. Consequently, the prototype filter varies slowly within the maximum channel delay spread. Thus, similar to [14], (5) can be written as

$$y^r_{\bar{m},\bar{n}} = \sum_{k=1}^{K} G^{r,k}_{\bar{m}} \Bigg(d^k_{\bar{m},\bar{n}} + \underbrace{\sum_{(m,n)\neq(\bar{m},\bar{n})} \frac{G^{r,k}_{m}}{G^{r,k}_{\bar{m}}} d^k_{m,n} \xi^{\bar{m},\bar{n}}_{m,n}}_{\text{Intrinsic Interference}} \Bigg) + \eta^r_{\bar{m},\bar{n}}, \tag{6}$$

where $G^{r,k}_{\bar{m}}$ represents the channel's frequency response (CFR) between the kth user and the rth BS antenna at the $\bar{m}$th subcarrier, which is expressed as $G^{r,k}_{\bar{m}} = \sum_{\tau=0}^{L_h-1} g_{r,k}[\tau] e^{\frac{-j2\pi\bar{m}\tau}{M}}$. The term $\eta^r_{\bar{m},\bar{n}} = \sum_{l=-\infty}^{\infty} \eta_r[l]\chi^*_{\bar{m},\bar{n}}[l]$ denotes the filtered version of the complex noise received at the rth BS antenna.

The total interference at the receiver is comprised of the ISI and the inter-carrier interference (ICI) at the point $(\bar{m}, \bar{n})$ in the FT lattice. Thanks to the well-localized FT prototype FBMC filter, only the first-order neighbor points of $(\bar{m}, \bar{n})$ within the FT lattice contribute significantly to the total interference, since the quantity $\xi^{\bar{m},\bar{n}}_{m,n}$ is negligible outside this first order neighborhood [5]. Additionally, the CFR is assumed to be constant over the first-order neighbor points of the FT lattice, which implies $G^{r,k}_{\bar{m}} \approx G^{r,k}_{m}$. By exploiting the above properties, (6) can be simplified to

$$y^r_{\bar{m},\bar{n}} = \sum_{k=1}^{K} G^{r,k}_{\bar{m}} b^k_{\bar{m},\bar{n}} + \eta^r_{\bar{m},\bar{n}}, \tag{7}$$

where $b^k_{\bar{m},\bar{n}} = d^k_{\bar{m},\bar{n}} + jI^k_{\bar{m},\bar{n}}$ is the virtual symbol corresponding to the kth user with its imaginary part representing the intrinsic interference $I^k_{\bar{m},\bar{n}} = \sum_{(m,n)\neq(\bar{m},\bar{n})} d^k_{m,n}\xi^{\bar{m},\bar{n}}_{m,n}$ [15]. The average power of the virtual symbol is expressed as $\mathbb{E}\big[b^k_{m,n}\big(b^k_{m,n}\big)^*\big] \approx 2P_k$ [18]. By concatenating the signals from all the received antennas at the BS, the vector representation of the FBMC/OQAM signal model is expressed as

$$\mathbf{y}_{\bar{m},\bar{n}} = \mathbf{G}_{\bar{m}}\mathbf{b}_{\bar{m},\bar{n}} + \boldsymbol{\eta}_{\bar{m},\bar{n}}, \tag{8}$$

where the entries of the vector $\mathbf{y}_{\bar{m},\bar{n}} = \big[y^1_{\bar{m},\bar{n}}, y^2_{\bar{m},\bar{n}}, \cdots, y^N_{\bar{m},\bar{n}}\big]^T \in \mathbb{C}^{N\times 1}$ represent the received signal across all the BS antennas and the (r,k)th element of the matrix $\mathbf{G}_{\bar{m}}$ is denoted by $G^{r,k}_{\bar{m}}$. The matrix $\mathbf{G}_{\bar{m}} = \mathbf{H}_{\bar{m}}\mathbf{D}^{1/2} = \big[\mathbf{g}^1_{\bar{m}}, \mathbf{g}^2_{\bar{m}}, \cdots, \mathbf{g}^K_{\bar{m}}\big] \in \mathbb{C}^{N\times K}$ is the uplink channel between the BS and users, where $\mathbf{H}_{\bar{m}}$ accounts for the small-scale fading having i.i.d elements and following the $\mathcal{CN}(0,1)$ distribution. Furthermore, the diagonal matrix $\mathbf{D} = \text{diag}(\beta_1, \beta_2, \cdots, \beta_K)$ accounts for the large-scale fading component [44]. The elements of the vector $\mathbf{b}_{\bar{m},\bar{n}} = \big[b^1_{\bar{m},\bar{n}}, b^2_{\bar{m},\bar{n}}, \cdots, b^K_{\bar{m},\bar{n}}\big]^T \in \mathbb{C}^{K\times 1}$ denote the virtual symbols of all the K users. The noise vector $\boldsymbol{\eta}_{\bar{m},\bar{n}} = \big[\eta^1_{\bar{m},\bar{n}}, \eta^2_{\bar{m},\bar{n}}, \cdots, \eta^N_{\bar{m},\bar{n}}\big]^T \in \mathbb{C}^{N\times 1}$ at the BS follows the distribution $\mathcal{CN}(\mathbf{0}, \sigma^2_\eta\mathbf{I}_N)$.

To detect the kth user signal, the BS combines its received signal $\mathbf{y}_{\bar{m},\bar{n}}$ using the linear combiner $\mathbf{w}^k_{\bar{m}}$. In this section, the BS is assumed to estimate the channel matrix $\mathbf{G}_{\bar{m}}$ and then uses it to design the receive combiner (RC) $\mathbf{w}^k_{\bar{m}}$. The vectors $\widehat{\mathbf{g}}^k_{\bar{m}}$ and $\mathbf{e}^k_{\bar{m}}$ denote the estimated version of $\mathbf{g}^k_{\bar{m}}$ and the channel estimation error, respectively. Upon exploiting $\mathbf{g}^k_{\bar{m}} = \widehat{\mathbf{g}}^k_{\bar{m}} + \mathbf{e}^k_{\bar{m}}$, the equivalent received signal after applying the RC in (8) can be expressed as

$$\begin{aligned}\big(\mathbf{w}^k_{\bar{m}}\big)^H\mathbf{y}_{\bar{m},\bar{n}} =& \big(\mathbf{w}^k_{\bar{m}}\big)^H\widehat{\mathbf{g}}^k_{\bar{m}} b^k_{\bar{m},\bar{n}} + \sum_{\substack{j=1\\ j\neq k}}^{K} \tilde{g}^j_{\bar{m}} b^j_{\bar{m},\bar{n}} \\ &+ \sum_{j=1}^{K} \tilde{e}^j_{\bar{m}} b^j_{\bar{m},\bar{n}} + \tilde{\eta}_{\bar{m},\bar{n}},\end{aligned} \tag{9}$$

where $\tilde{g}^j_{\bar{m}} = (\mathbf{w}^k_{\bar{m}})^H\widehat{\mathbf{g}}^j_{\bar{m}}$, $\tilde{e}^j_{\bar{m}} = (\mathbf{w}^k_{\bar{m}})^H\mathbf{e}^j_{\bar{m}}$ and $\tilde{\eta}_{\bar{m},\bar{n}} = (\mathbf{w}^k_{\bar{m}})^H\boldsymbol{\eta}_{\bar{m},\bar{n}}$. The estimated version of the OQAM transmitted signal for the kth user, over index $(\bar{m}, \bar{n})$ at the receiver, can be expressed as

$$\widehat{d}^k_{\bar{m},\bar{n}} = \Re\{\big(\mathbf{w}^k_{\bar{m}}\big)^H\mathbf{y}_{\bar{m},\bar{n}}\} = \Re\Big\{\big(\mathbf{w}^k_{\bar{m}}\big)^H\widehat{\mathbf{g}}^k_{\bar{m}} b^k_{\bar{m},\bar{n}}\Big\} + \vartheta^k_{\bar{m},\bar{n}}, \tag{10}$$

where the first and second terms in (10) represent the desired and interference-plus-noise signal at the receiver, respectively. The expression $\vartheta^k_{\bar{m},\bar{n}} = \Re\big\{\sum_{\substack{j=1\\ j\neq k}}^{K} \tilde{g}^j_{\bar{m}} b^j_{\bar{m},\bar{n}} + \sum_{j=1}^{K} \tilde{e}^j_{\bar{m}} b^j_{\bar{m},\bar{n}} + \tilde{\eta}_{\bar{m},\bar{n}}\big\}$ represents the combined effect of multi-user interference, channel estimation error and AWGN noise at the receiver.

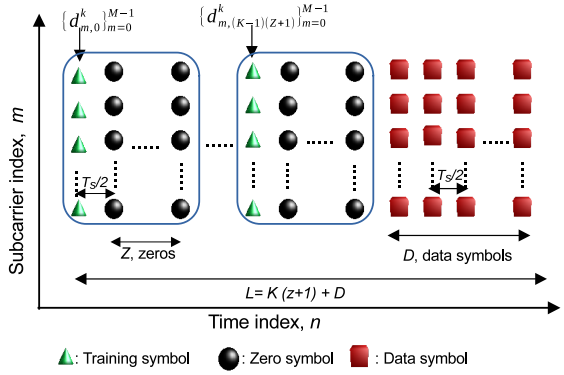

Fig. 1: FBMC/OQAM frame structure for the kth user

B. Channel estimation

Since the basis functions of FBMC/OQAM systems are only orthogonal in the real-domain, the procedure of channel estimation is different from that of OFDM, owing to the associated intrinsic interference [49]. This section determines the MMSE estimate of the CFR matrix $\mathbf{G}_{\bar{m}}$. It can be readily observed from (8) that to estimate the $N \times K$ CFR matrix $\mathbf{G}_{\bar{m}}$, each user is required to transmit at least K non-zero pilot symbols. The frame structure of each user is shown in Fig. 1. Let $L = (z+1)K + D$ denote the number of symbols transmitted by each user at each subcarrier, where K denotes the number of training symbols and D is the number of data symbols. In contrast to OFDM, the adjacent FBMC symbols overlap with each other in the TD because of the overlapping nature of the prototype filter. Hence, z zeros are placed between the adjacent training symbols to mitigate the ISI [49].

For channel estimation, (8) is evaluated at the pilot locations $\bar{n} = 0, (z+1), \cdots, (z+1)(K-1)$ and the corresponding observation vectors $\mathbf{y}_{\bar{m},0}, \mathbf{y}_{\bar{m},(z+1)}, \cdots, \mathbf{y}_{\bar{m},(K-1)(z+1)}$ are collected in the observation matrix $\mathbf{Y}_{\bar{m}} = \left[\mathbf{y}_{\bar{m},0}, \mathbf{y}_{\bar{m},(z+1)}, \cdots \mathbf{y}_{\bar{m},(z+1)(K-1)}\right] \in \mathbb{C}^{N\times K}$, which is expressed as

$$\mathbf{Y}_{\bar{m}} = \mathbf{G}_{\bar{m}}\mathbf{B}_{\bar{m}} + \boldsymbol{\eta}_{\bar{m}}, \tag{11}$$

where $\boldsymbol{\eta}_{\bar{m}} = [\boldsymbol{\eta}_{\bar{m},0}, \boldsymbol{\eta}_{\bar{m},(z+1)}, \cdots, \boldsymbol{\eta}_{\bar{m},(z+1)(K-1)}] \in \mathbb{C}^{N\times K}$ represents the noise matrix. The pilot matrix is represented as $\mathbf{B}_{\bar{m}} = [\tilde{\mathbf{b}}^1_{\bar{m}}, \tilde{\mathbf{b}}^2_{\bar{m}}, \cdots, \tilde{\mathbf{b}}^K_{\bar{m}}]^T$, where $(\tilde{\mathbf{b}}^k_{\bar{m}})^T$ denotes the pilot vector for the kth user so that we have $(\tilde{\mathbf{b}}^k_{\bar{m}})^T(\tilde{\mathbf{b}}^j_{\bar{m}})^* = P_p$ for $j = k$ and it is equal to 0 for $j \neq k$, because $\mathbf{B}_{\bar{m}}$ is the orthogonal, i.e, we have $\mathbf{B}_{\bar{m}}\mathbf{B}^H_{\bar{m}} = P_p\mathbf{I}_K$ [50]. To estimate the channel vector $\mathbf{g}^k_{\bar{m}}$ of the kth user at the $\bar{m}$th subcarrier, the output matrix $\mathbf{Y}_{\bar{m}}$ is multiplied by $\left(\tilde{\mathbf{b}}^k_{\bar{m}}\right)^*$ to obtain $\mathbf{y}^k_{\bar{m}} \in \mathbb{C}^{N\times 1}$ as shown below

$$\mathbf{y}^k_{\bar{m}} = \mathbf{Y}_{\bar{m}}\left(\tilde{\mathbf{b}}^k_{\bar{m}}\right)^* = P_p\mathbf{g}^k_{\bar{m}} + \boldsymbol{\eta}^k_{\bar{m}}, \tag{12}$$

where $\mathbf{g}^k_{\bar{m}} = (\beta_k)^{\frac{1}{2}}\mathbf{h}^k_{\bar{m}}$ and $\boldsymbol{\eta}^k_{\bar{m}} = \boldsymbol{\eta}_{\bar{m}}(\tilde{\mathbf{b}}^k_{\bar{m}})^*$ upon using (12), the MMSE channel estimate of $\mathbf{g}^k_{\bar{m}}$ is derived as [50] $\widehat{\mathbf{g}}^k_{\bar{m}} = \mathbf{R}_{\mathbf{g}^k_{\bar{m}}\mathbf{y}^k_{\bar{m}}}\mathbf{R}^{-1}_{\mathbf{y}^k_{\bar{m}}\mathbf{y}^k_{\bar{m}}}\mathbf{y}^k_{\bar{m}}$, where $\mathbf{R}_{\mathbf{g}^k_{\bar{m}}\mathbf{y}^k_{\bar{m}}} = P_p\beta_k\mathbf{I}_N$ and $\mathbf{R}_{\mathbf{y}^k_{\bar{m}}\mathbf{y}^k_{\bar{m}}} = ({P_p}^2\beta_k + p_p{\sigma_\eta}^2)\mathbf{I}_N$ are the cross-covariance and auto-covariance matrices. By exploiting these properties, the channel estimate for the kth user can be obtained as $\widehat{\mathbf{g}}^k_{\bar{m}} = \frac{\beta_k}{(P_p\beta_k+\sigma_\eta{}^2)}\mathbf{y}^k_{\bar{m}}$. The covariance matrices of the channel estimate $\widehat{\mathbf{g}}^k_{\bar{m}}$ and the estimation error $\mathbf{e}^k_{\bar{m}}$ are calculated as $\mathbb{E}\left[\widehat{\mathbf{g}}^k_{\bar{m}}(\widehat{\mathbf{g}}^k_{\bar{m}})^H\right] = \frac{P_p(\beta_k)^2}{(P_p\beta_k+\sigma_\eta{}^2)}\mathbf{I}_N$ and $\mathbb{E}\left[\mathbf{e}^k_{\bar{m}}(\mathbf{e}^k_{\bar{m}})^H\right] = \frac{\beta_k\sigma^2_\eta}{(P_p\beta_k+\sigma_\eta{}^2)}\mathbf{I}_N$.

III. Achievable Spectral Efficiency

This section derives the closed-form SE expressions characterizing the FBMC/OQAM uplink of massive MIMO systems. The expressions derived are applicable for any number of BS antennas and depend only on the large-scale characteristics. This helps the system designer calculate the SE without the need to perform time consuming system level simulations. To begin with, the uplink ergodic SE expressions are explicitly determined for the MRC and ZF receivers.

1) MRC receiver

For the MRC combiner vector $\mathbf{w}^k_{\bar{m}} = \widehat{\mathbf{g}}^k_{\bar{m}}$ in (10) that is constructed using the estimated CSI, the estimate of the transmitted OQAM signal of the kth user at the $(\bar{m},\bar{n})$ index can be expressed as $\widehat{d}^k_{\bar{m},\bar{n}} = \Re\{(\widehat{\mathbf{g}}^k_{\bar{m}})^H\mathbf{y}_{\bar{m},\bar{n}}\} = \Re\{\|\widehat{\mathbf{g}}^k_{\bar{m}}\|^2 b^k_{\bar{m},\bar{n}}\} + \vartheta^{k,\text{MRC}}_{\bar{m},\bar{n}}$, where $\vartheta^{k,\text{MRC}}_{\bar{m},\bar{n}} = \Re\{\sum_{\substack{j=1\\j\neq k}}^{K}(\widehat{\mathbf{g}}^k_{\bar{m}})^H\widehat{\mathbf{g}}^j_{\bar{m}}b^j_{\bar{m},\bar{n}} + \sum_{j=1}^{K}(\widehat{\mathbf{g}}^k_{\bar{m}})^H\mathbf{e}^j_{\bar{m}}b^j_{\bar{m},\bar{n}} + (\widehat{\mathbf{g}}^k_{\bar{m}})^H\boldsymbol{\eta}_{\bar{m},\bar{n}}\}$ represents the interference-plus-noise at the receiver. The uplink ergodic SE achieved with MRC combining at the BS can be expressed as

$$R^{\text{MRC}}_{\bar{m}} = \frac{\tau_d}{T}\sum_{k=1}^{K}\mathbb{E}\left[\log_2\left(1+\text{SINR}^{\text{MRC}}_{\bar{m},k}\right)\right], \text{ with} \tag{13}$$

$$\text{SINR}^{\text{MRC}}_{\bar{m},k} = \frac{P_k\left\|\widehat{\mathbf{g}}^k_{\bar{m}}\right\|^4}{\sum\limits_{\substack{j=1\\j\neq k}}^{K}P_j\left|\left(\widehat{\mathbf{g}}^k_{\bar{m}}\right)^H\widehat{\mathbf{g}}^j_{\bar{m}}\right|^2 + \sum\limits_{j=1}^{K}P_j\left|\left(\widehat{\mathbf{g}}^k_{\bar{m}}\right)^H\mathbf{e}^j_{\bar{m}}\right|^2 + \|\widehat{\mathbf{g}}^k_{\bar{m}}\|^2\frac{\sigma^2_\eta}{2}}, \tag{14}$$

where $\text{SINR}^{\text{MRC}}_{\bar{m},k}$ denotes the SINR expression of the kth user at the BS. The detailed steps of deriving the power of $\vartheta^{k,\text{MRC}}_{\bar{m},\bar{n}}$, which forms the denominator of (14), are provided in Appendix A (refer to (42)). The pre-log factor $\frac{\tau_d}{T}$ in (13) denotes the pilot overhead arising due to channel estimation.

2) ZF receiver

The output signal upon applying the ZF combiner matrix $\mathbf{W}^k_{\bar{m}} = (\widehat{\mathbf{G}}^\dagger_{\bar{m}})^H = \widehat{\mathbf{G}}_{\bar{m}}(\widehat{\mathbf{G}}^H_{\bar{m}}\widehat{\mathbf{G}}_{\bar{m}})^{-1} \in \mathbb{C}^{N\times K}$ can be expressed as $\widehat{\mathbf{G}}^\dagger_{\bar{m}}\mathbf{y}_{\bar{m},\bar{n}} = \mathbf{b}_{\bar{m},\bar{n}} + \widehat{\mathbf{G}}^\dagger_{\bar{m}}\mathbf{E}_{\bar{m}}\mathbf{b}_{\bar{m},\bar{n}} + \widehat{\mathbf{G}}^\dagger_{\bar{m}}\boldsymbol{\eta}_{\bar{m},\bar{n}}$, where $\widehat{\mathbf{G}}_{\bar{m}} = \left[\widehat{\mathbf{g}}^1_{\bar{m}}, \widehat{\mathbf{g}}^2_{\bar{m}}, \cdots, \widehat{\mathbf{g}}^K_{\bar{m}}\right] \in \mathbb{C}^{N\times K}$ and $\mathbf{E}_{\bar{m}} = \left[\mathbf{e}^1_{\bar{m}}, \mathbf{e}^2_{\bar{m}}, \cdots, \mathbf{e}^K_{\bar{m}}\right] \in \mathbb{C}^{N\times K}$ represent the channel estimate and channel estimation error matrices, respectively. The estimate of the OQAM signal vector $\mathbf{d}_{\bar{m},\bar{n}} = \left[d^1_{\bar{m},\bar{n}}, d^2_{\bar{m},\bar{n}}, \cdots, d^K_{\bar{m},\bar{n}}\right]^T \in \mathbb{C}^{K\times 1}$ at the BS can be expressed as $\widehat{\mathbf{d}}_{\bar{m},\bar{n}} = \Re\{\widehat{\mathbf{G}}^\dagger_{\bar{m}}\mathbf{y}_{\bar{m},\bar{n}}\} = \mathbf{d}_{\bar{m},\bar{n}} + \boldsymbol{\vartheta}^{\text{ZF}}_{\bar{m},\bar{n}}$, where the vector $\boldsymbol{\vartheta}^{\text{ZF}}_{\bar{m},\bar{n}} = \Re\{\widehat{\mathbf{G}}^\dagger_{\bar{m}}\mathbf{E}_{\bar{m}}\mathbf{b}_{\bar{m},\bar{n}} + \widehat{\mathbf{G}}^\dagger_{\bar{m}}\boldsymbol{\eta}_{\bar{m},\bar{n}}\} \in \mathbb{C}^{K\times 1}$ represents the interference-plus-noise vector at the BS. The ergodic uplink SE, therefore, is given by

$$R^{\text{ZF}}_{\bar{m}} = \frac{\tau_d}{T}\sum_{k=1}^{K}\mathbb{E}\left[\log_2\left(1+\text{SINR}^{\text{ZF}}_{\bar{m},k}\right)\right], \text{ with} \tag{15}$$

$$\text{SINR}_{\bar{m},k}^{\text{ZF}}=\frac{P_k}{\left\{\begin{array}{l}\left[(\widehat{\mathbf{G}}_{\bar{m}}^H\widehat{\mathbf{G}}_{\bar{m}})^{-2}\right]_{k,k}\left((\widehat{\mathbf{g}}_{\bar{m}}^k)^H\left(\sum_{j=1}^{K}P_j\mathbf{e}_{\bar{m}}^j(\mathbf{e}_{\bar{m}}^j)^H\right)\widehat{\mathbf{g}}_{\bar{m}}^k\right)\\+\left[(\widehat{\mathbf{G}}_{\bar{m}}^H\widehat{\mathbf{G}}_{\bar{m}})^{-1}\right]_{k,k}\frac{\sigma_\eta^2}{2}\end{array}\right\}},\quad \overline{\text{SINR}}_{\bar{m},k}^{\text{MRC}}=\frac{P_k\left|\mathbb{E}\left[(\widehat{\mathbf{g}}_{\bar{m}}^k)^H\mathbf{g}_{\bar{m}}^k\right]\right|^2}{\left\{\begin{array}{l}P_k\text{Var}\left[(\widehat{\mathbf{g}}_{\bar{m}}^k)^H\mathbf{g}_{\bar{m}}^k\right]+\sum_{\substack{j=1\\j\neq k}}^{K}P_j\mathbb{E}\left[\left|(\widehat{\mathbf{g}}_{\bar{m}}^k)^H\mathbf{g}_{\bar{m}}^j\right|^2\right]\\+\mathbb{E}\left[\|\widehat{\mathbf{g}}_{\bar{m}}^k\|^2\right]\frac{\sigma_\eta^2}{2}\end{array}\right\}}\triangleq\frac{\text{N}_{\bar{m},k}^{\text{MRC}}(\mathbf{p})}{\text{D}_{\bar{m},k}^{\text{MRC}}(\mathbf{p})}. \tag{16, 20}$$

where $\text{SINR}_{\bar{m},k}^{\text{ZF}}$ denotes the SINR expression of the kth user at the BS. The detailed derivation of the covariance matrix of $\boldsymbol{\vartheta}_{\bar{m},\bar{n}}^{\text{ZF}}$, which is required for obtaining (16), is provided in Appendix B (refer to (44)). Note that due to the expectation operator outside the logarithm, it is difficult to further simplify the SE expressions in (13) and (15). Exploiting the UatF bound [44], a closed-form expression for the proposed FBMC-based massive MIMO system has been derived, which holds for an arbitrary number of BS antennas. To achieve this aim, (9) can be re-written as follows

$$\begin{aligned}\left(\mathbf{w}_{\bar{m}}^k\right)^H\mathbf{y}_{\bar{m},\bar{n}}=&\mathbb{E}\left[\left(\mathbf{w}_{\bar{m}}^k\right)^H\mathbf{g}_{\bar{m}}^k\right]b_{\bar{m},\bar{n}}^k+\left(\left(\mathbf{w}_{\bar{m}}^k\right)^H\mathbf{g}_{\bar{m}}^k-\mathbb{E}\left[\left(\mathbf{w}_{\bar{m}}^k\right)^H\mathbf{g}_{\bar{m}}^k\right]\right)b_{\bar{m},\bar{n}}^k\\&+\sum_{\substack{j=1\\j\neq k}}^{K}\left(\mathbf{w}_{\bar{m}}^k\right)^H\mathbf{g}_{\bar{m}}^jb_{\bar{m},\bar{n}}^j+\left(\mathbf{w}_{\bar{m}}^k\right)^H\boldsymbol{\eta}_{\bar{m},\bar{n}}.\end{aligned} \tag{17}$$

The received signal in (10) can be expressed as

$$\begin{aligned}\widehat{d}_{\bar{m},\bar{n}}^k&=\Re\left\{\left(\mathbf{w}_{\bar{m}}^k\right)^H\mathbf{y}_{\bar{m},\bar{n}}\right\}\\&=\underbrace{\Re\left\{\mathbb{E}\left[\left(\mathbf{w}_{\bar{m}}^k\right)^H\mathbf{g}_{\bar{m}}^k\right]b_{\bar{m},\bar{n}}^k\right\}}_{\text{Desired Signal}}+\underbrace{\overline{\vartheta}_{\bar{m},\bar{n}}^k}_{\text{Effective Noise}},\end{aligned}$$

where

$$\begin{aligned}\overline{\vartheta}_{\bar{m},\bar{n}}^k=&\underbrace{\Re\left\{\left(\left(\mathbf{w}_{\bar{m}}^k\right)^H\mathbf{g}_{\bar{m}}^k-\mathbb{E}\left[\left(\mathbf{w}_{\bar{m}}^k\right)^H\mathbf{g}_{\bar{m}}^k\right]\right)b_{\bar{m},\bar{n}}^k\right\}}_{\text{Beamforming Uncertainty}}\\&+\underbrace{\Re\left\{\sum_{\substack{j=1\\j\neq u}}^{U}\left(\mathbf{w}_{\bar{m}}^k\right)^H\mathbf{g}_{\bar{m}}^jb_{\bar{m},\bar{n}}^j\right\}}_{\text{Multi-user interference}}+\underbrace{\Re\left\{\left(\mathbf{w}_{\bar{m}}^k\right)^H\boldsymbol{\eta}_{\bar{m},\bar{n}}\right\}}_{\text{Noise}}.\end{aligned} \tag{18}$$

The desired signal term and all the other terms of the effective noise $\overline{\vartheta}_{\bar{m},\bar{n}}^k$ can be shown to be uncorrelated. For massive MIMO systems, since the effective noise is comprised of the sum of a large number of terms, upon invoking the central limit theorem, it can be approximated by Gaussian noise [43]. The closed-form expressions derived next in Theorem 1 and Theorem 2, provide a tight lower bound on the ergodic SE, as shown numerically in Section V.

Theorem 1. The ergodic SE of an uplink FBMC/OQAM system for a finite number of antennas at the BS, relying on the MMSE channel estimate based MRC receiver (i.e. $\mathbf{w}_{\bar{m}}^k=\widehat{\mathbf{g}}_{\bar{m}}^k$), is lower-bounded as

$$\overline{R}_{\bar{m}}^{\text{MRC}}=\frac{\tau_d}{T}\sum_{k=1}^{K}\log_2\left(1+\overline{\text{SINR}}_{\bar{m},k}^{\text{MRC}}\right),\ \text{with} \tag{19}$$

Proof. The detailed derivation of the above expression is provided in Appendix C (refer to (49)). Unlike the $\text{SINR}_{\bar{m},k}^{\text{MRC}}$ in (14), the terms of $\overline{\text{SINR}}_{\bar{m},k}^{\text{MRC}}$ in (20) are statistical quantities that can be derived in closed-form. The detailed procedure of deriving the closed-form expression of $\overline{\text{SINR}}_{\bar{m},k}^{\text{MRC}}$ is given in Appendix C. □

Theorem 2. The ergodic SE of an uplink FBMC/OQAM system for a finite number of antennas at the BS, relying on the MMSE channel estimate based ZF receiver (i.e. $\mathbf{W}_{\bar{m}}^k=(\widehat{\mathbf{G}}_{\bar{m}}^\dagger)^H=\widehat{\mathbf{G}}_{\bar{m}}(\widehat{\mathbf{G}}_{\bar{m}}^H\widehat{\mathbf{G}}_{\bar{m}})^{-1}$), is lower-bounded by

$$\overline{R}_{\bar{m}}^{\text{ZF}}=\frac{\tau_d}{T}\sum_{k=1}^{K}\log_2\left(1+\overline{\text{SINR}}_{\bar{m},k}^{\text{ZF}}\right),\ \text{with} \tag{22}$$

$$\overline{\text{SINR}}_{\bar{m},k}^{\text{ZF}}=\frac{P_k}{\left\{\begin{array}{l}\left(\sum_{j=1}^{K}P_j\mathbb{E}\left[e_{\bar{m}}^j(e_{\bar{m}}^j)^*\right]+\frac{\sigma_\eta^2}{2}\right)\\\times\mathbb{E}\left[\{(\widehat{\mathbf{G}}_{\bar{m}}^H\widehat{\mathbf{G}}_{\bar{m}})^{-1}\}_{k,k}\right]\end{array}\right\}}\triangleq\frac{\text{N}_{\bar{m},k}^{\text{ZF}}(\mathbf{p})}{\text{D}_{\bar{m},k}^{\text{ZF}}(\mathbf{p})}. \tag{23}$$

where $\overline{\text{SINR}}_{\bar{m},k}^{\text{ZF}}$ denotes the SINR of the kth user at subcarrier index $\bar{m}$.

Proof. The detailed derivation of the result in (23) is provided in Appendix D (refer to (60)). Unlike (16), the terms of $\overline{\text{SINR}}_{\bar{m},k}^{\text{ZF}}$ in (23) are statistical quantities. After further simplification, they result in the closed-form expression of $\overline{\text{SINR}}_{\bar{m},k}^{\text{ZF}}$ for which the detailed procedure is shown in Appendix D. □

IV. EMF Aware Global Energy Efficiency (GEE) Optimization

This section proposes an algorithm for maximizing the GEE of an FBMC massive MIMO system. Furthermore, to account for the health risks associated with EMF emissions, the EMF exposure constraints are taken into consideration for the energy-efficient design. The GEE, measured in bits/Joule, is a network-centric metric that is defined as the fraction of the network throughput (product of SE and bandwidth) to the total power consumed [44]. Recall that the closed-form SE expressions described in Theorem 1 and 2 only require long-term statistics of the channel. The GEE can therefore be formulated as

$$f_{\text{GEE}}=\frac{B\times\frac{\tau_d}{T}\sum_{k=1}^{K}\log_2\left(1+\overline{\text{SINR}}_{\bar{m},k}^{\Delta}\right)}{\frac{\tau_d}{T}\sum_{k=1}^{K}\upsilon_{\text{PA},k}^{-1}P_k+\frac{\tau_p}{T}\sum_{k=1}^{K}\upsilon_{\text{PA},k}^{-1}P_{p,k}+P_c}. \tag{24}$$

Here B denotes the bandwidth, and the constant $\upsilon_{\text{PA},k} \in (0,1]$ represents the power amplifier (PA) efficiency at the user. The first and second terms in the denominator denote the power consumption during the data transmission and channel estimation phases, respectively, and the third term denotes the total circuit power dissipation [44].

Power Consumption: The quantity P_c represents the circuit power comprised of the power consumed by the analog and digital circuitry of the transceiver. It is calculated as $P_c = P_{\text{FIX}} + P_{\text{TX}} + P_{\text{CE}} + P_{\text{SP}}$ [44]. The term P_{FIX} denotes the fixed component of the circuit power required for baseband signal processing, controlling, and site-cooling. The term P_{TX} denotes the power consumed by the transceiver blocks and it is expressed as $P_{\text{TX}} = P_{\text{LO}} + NP_{\text{BS}} + KP_{\text{UE}}$, where the terms P_{LO}, P_{BS} and P_{UE} denote the power required by the local oscillator, the circuit connected to each antenna at the BS and the user equipment, respectively. The remaining power terms P_{SP} and P_{CE}, computed similarly to [44, sec. 5.4], denote the power dissipated by the signal processing and channel estimation modules at the user/BS, respectively.

Existing works on massive MIMO-FBMC system design [45], [46], allocate equal power to the users and do not include the effect of electromagnetic exposure. By contrast, this work maximizes the GEE considering both the transmit power and SAR constraints, which ensure that there is no health risk posed by EM radiation. Therefore, the optimization problem to maximize the GEE can be formulated as

$$\textbf{P1:} \quad \max_{\mathbf{p}} \quad \frac{B \times \frac{\tau_d}{T} \sum_{k=1}^{K} \log_2\left(1 + \overline{\text{SINR}}_{\bar{m},k}^{\Delta}\right)}{\mathcal{P}_{\text{tot}}(\mathbf{p})} \tag{25a}$$

$$\text{s.t.} \quad 0 \le P_k \le P_k^{\max}, \quad \forall k, \tag{25b}$$

$$SAR_{ref} P_k \le q_k, \quad \forall k. \tag{25c}$$

The quantity $\mathcal{P}_{\text{tot}}(\mathbf{p}) = \frac{\tau_d}{T}\sum_{k=1}^{K} \upsilon_{\text{PA},k}^{-1} P_k + \frac{\tau_p}{\tau}\upsilon_{\text{PA}}^{-1}\sum_{k=1}^{K} P_{p,k} + P_c$ represents the total network power consumption. The constraint in (25b) limits the transmit power of each user to $P_k^{\max}$. The transmit power is also restricted to limit the uplink EM exposure of the user by imposing the SAR constraint in (25c), where $\{q_k\}_{k=1}^{K}$ and $\{SAR_{ref}\}_{k=1}^{K}$ denote the SAR thresholds and the SAR reference values, respectively [35], [39]. The scalars $\{q_k\}_{k=1}^{K}$, measured in Watt/kg, limit the maximum allowed exposition to EM radiation, as imposed by the regulatory agencies (FCC, ICNIRP) [29], [31]. The quantities $\{SAR_{ref}\}_{k=1}^{K}$ measure the rate at which the EM energy is absorbed by the human body per unit watt of transmitted power. This work adopted the standard exposure model proposed in [30] for the assessment of EMF exposure at each user device. The above-said model takes into account various factors that determine exposure, such as population age group, duration of exposure, usage type (voice/data), exposed body part (head for voice users, wrist/torso for data users), and network type (Global System for Mobile Communications/Long-Term Evolution/WiFi).

The GEE objective in **P1** is a single-ratio fractional program, with the numerator denoting the networks SE and the denominator denoting the networks total power consumption. It can be observed that the SE is the sum of the log-ratios that are rational functions of the optimization variables, which renders the aforementioned GEE maximization problem non-convex. Consequently, it is challenging to solve **P1**, which is further complicated by the constraints in (25b) and (25c). In the next two sub-sections, novel techniques are proposed relying on the nested quadratic transform and Lagrangian dual transform (LDT) frameworks to attain the optimal solution of the above GEE maximization problem. The NQT framework applies a quadratic transform to recast the multiple ratio network SE nested with a single-ratio GEE objective as quadratic concave function. A fixed-point closed-form solution of the GEE maximization problem is presented next using the LDT framework.

A. GEE optimization via nested quadratic transform (NQT)

The QT framework is typically applied to problems comprising ratios of optimization variables, and it is based on replacing the non-convex ratio terms in the original problem by concave functions [51]. The QT was originally stated in the following lemma [51, Corollary 2].

Lemma 1. Given a sequence of non-decreasing functions f_k and sequence of ratios $A_k(\mathbf{x})/B_k(\mathbf{x})$ such that $A_k(\mathbf{x}) : \mathbb{R}^d \to \mathbb{R}_+$ and $B_k(\mathbf{x}) : \mathbb{R}^d \to \mathbb{R}_{++}$ for $k = 1, 2, \cdots, K$, the sum of the functions of the ratio problem is

$$\max_{\mathbf{x}} \quad \sum_{k=1}^{K} f_k\left(\frac{A_k(\mathbf{x})}{B_k(\mathbf{x})}\right) \quad \text{s.t. } \mathbf{x} \in \mathcal{X}.$$

The above optimization problem can, therefore, be equivalently reformulated as

$$\max_{\mathbf{x},\mathbf{y}} \quad \sum_{k=1}^{K} f_k\left(2y_k\sqrt{A_k(\mathbf{x})} - y_k^2 B_k(\mathbf{x})\right)$$
$$\text{s.t. } \mathbf{x} \in \mathcal{X},\ y_k \in \mathbb{R}, \text{ for } \forall k,$$

where $\mathbf{x}$ is an optimization variable, $\mathcal{X}$ is a convex set and $\mathbf{y}$ is the collection of the auxiliary variables $\{y_1, y_2, \cdots, y_K\}$ that decouple the numerator and denominator of the inner ratio $A_k(\mathbf{x})/B_k(\mathbf{x})$ of the original optimization problem. Interestingly, the equivalent problem can be solved iteratively over the optimization variable $\mathbf{x}$ and auxiliary variable $\mathbf{y}$. For a fixed $\mathbf{x}$, the auxiliary variable $\mathbf{y}$ can be updated as $y_k^* = \frac{\sqrt{A_k(\mathbf{x})}}{B_k(\mathbf{x})}$.

The constant B is ignored in (25a), and the problem **P1** is recast using Lemma 1. The numerator of the GEE objective $\overline{R}_{\bar{m}}^{\Delta} = \frac{\tau_d}{T}\sum_{k=1}^{K}\log_2\left(1 + \overline{\text{SINR}}_{\bar{m},k}^{\Delta}\right)$ is a non-decreasing function defined over $\mathbb{R}_+$, while the denominator $\mathcal{P}_{\text{tot}}(\mathbf{p})$ is an affine function defined over $\mathbb{R}_{++}$. The numerator and denominator of the GEE objective, using the QT, are decoupled by introducing the auxiliary variable $z_{\bar{m}}^{\Delta}$. Thus, the optimization problem **P1** can be rewriten as follows

$$\textbf{P2:} \max_{\mathbf{p}, z_{\bar{m}}^{\Delta}} f_{\mathcal{Q}1}\left(\mathbf{p}, z_{\bar{m}}^{\Delta}\right) = 2z_{\bar{m}}^{\Delta} \times \sqrt{\frac{\tau_d}{T}\sum_{k=1}^{K}\log_2\left(1 + \overline{\text{SINR}}_{\bar{m},k}^{\Delta}\right)} - {z_{\bar{m}}^{\Delta}}^2\left(\mathcal{P}_{\text{tot}}(\mathbf{p})\right), \tag{26a}$$

$$\text{s.t. } z_{\bar{m}}^{\Delta} \in \mathbb{R}, 0 \le P_k \le \min\left(P_k^{\max}, \frac{q_k}{SAR_{ref}}\right), \forall k, \tag{26b}$$

where the second constraint in (26b) represents the single power constraint obtained by combining (25b) and (25c). It can be verified that when $\mathbf{p}$ is fixed, the objective in **P2** is a concave function of $z_{\bar{m}}^{\Delta}$. The optimal value of $z_{\bar{m}}^{\Delta}$ can, therefore, be obtained by setting $\partial f_{\mathcal{Q}1}(\mathbf{p}, z_{\bar{m}}^{\Delta})/\partial z_{\bar{m}}^{\Delta}$ to zero as

$$z_{\bar{m}}^{\Delta} = \frac{\sqrt{\frac{\tau_d}{T}\sum_{k=1}^{K}\log_2\left(1+\overline{\mathrm{SINR}}_{\bar{m},k}^{\Delta}\right)}}{\mathcal{P}_{\mathrm{tot}}(\mathbf{p})}. \tag{27}$$

The first term of the objective in **P2** is a concave function, provided that the terms inside the square-root, i.e., $\sum_{k=1}^{K}\log_2\left(1+\overline{\mathrm{SINR}}_{\bar{m},k}^{\Delta}\right)$, are also concave functions. Since the quantities $\overline{\mathrm{SINR}}_{\bar{m},k}^{\Delta}$ in (20) and (23) are in fractional form, the optimization problem **P2** is still non-convex over $\mathbf{p}$. Applying Lemma 1 once again to each of the $\overline{\mathrm{SINR}}_{\bar{m},k}^{\Delta}$ terms of **P2**, the equivalent optimization problem can be recast as

$$\textbf{P3:} \underset{\mathbf{p}^k, \mathbf{y}_{\bar{m}}^{\Delta}, z_{\bar{m}}^{\Delta}}{\mathrm{Max}} \quad f_{\mathcal{Q}2}(\mathbf{p}, \mathbf{y}_{\bar{m}}^{\Delta}, z_{\bar{m}}^{\Delta}) = 2z_{\bar{m}}^{\Delta} \times \sqrt{\frac{\tau_d}{T}\sum_{k=1}^{K}\log_2\left(1+2y_{\bar{m},k}^{\Delta}\sqrt{\mathrm{N}_{\bar{\mathrm{m}},\mathrm{k}}^{\Delta}(\mathbf{p})}-(y_{\bar{m},k}^{\Delta})^2\mathrm{D}_{\bar{m},k}^{\Delta}(\mathbf{p})\right)} - {z_{\bar{m}}^{\Delta}}^2\left(\mathcal{P}_{\mathrm{tot}}(\mathbf{p})\right), \tag{28a}$$

$$\text{s.t.} \quad y_{\bar{m},k}^{\Delta} \in \mathbb{R}, \text{(26b)}. \tag{28b}$$

The auxiliary variables $\mathbf{y}_{\bar{m}}^{\Delta} = \left[y_{\bar{m},1}^{\Delta}, y_{\bar{m},2}^{\Delta}, \cdots, y_{\bar{m},k}^{\Delta}\right]^T$ decouple the ratio of the $\overline{\mathrm{SINR}}_{\bar{m},k}^{\Delta}$ terms in $f_{\mathcal{Q}1}(\mathbf{p}, z_{\bar{m}}^{\Delta})$ in (26a). The optimal value of the $y_{\bar{m},k}^{\Delta}$ is updated iteratively as

$$y_{\bar{m},k}^{\Delta} = \frac{\sqrt{\mathrm{N}_{\bar{m},k}^{\Delta}(\mathbf{p})}}{\mathrm{D}_{\bar{m},k}^{\Delta}(\mathbf{p})}. \tag{29}$$

For fixed auxiliary variables $(z_{\bar{m}}^{\Delta}, \mathbf{y}_{\bar{m}}^{\Delta})$, the problem **P3** is concave over $\mathbf{p}$ and can be readily solved to determine the optimal $\mathbf{p}$ using any standard toolbox, such as the popular CVX [52]. The auxiliary variables are calculated using (27) and (29). This process is repeated until the objective in **P3** converges to a stationary point of **P1**. The various steps of the NQT approach for EMF aware GEE maximization are summarized in Algorithm 1, which computes $\left\{y_{\bar{m},k}^{\Delta}\right\}_{k=1}^{K}$ and $z_{\bar{m}}^{\Delta}$ in step 2 and solves problem **P3** in step 3. The worst-case computational complexity of the Algorithm 1 is dominant by computing power variable $\mathbf{p}$. Since a convex problem needs to be solved at each iteration, this approach ends up with large computational complexity (refer to Subsection IV-C), which renders it impractical. To reduce this complexity, a computationally efficient closed-form solution for EMF aware GEE optimization algorithm is proposed next that exploits the Lagrangian dual transform to iteratively update the optimization variables [53].

Algorithm 1: EMF aware GEE maximization Algorithm using the NQT

Input: Given a tolerance $\epsilon > 0$, SAR Threshold $\{q_k\}_{k=1}^{K}$ and reference SAR $\{SAR_{ref}\}_{k=1}^{K}$. Initialize $\left\{P_k\right\}_{k=1}^{K}$ with equal power allocation i.e., $\left\{P_k{}^{(0)}\right\}_{k=1}^{K} = \frac{P_k^{\max}}{K}$. Initialize $f_{\mathrm{GEE}}{}^{(0)} = f_{\mathrm{GEE}}(\mathbf{p}^{(0)})$. Set $i = 0$.

Output: $\mathbf{p}^* = \left\{P_k{}^*\right\}_{k=1}^{K}$ as the solutions.

1 **while** $\|f_{\mathrm{GEE}}{}^{(i+1)} - f_{\mathrm{GEE}}{}^{(i)}\| > \epsilon$

2 Given a feasible $\mathbf{p}^{(i)}$, compute the auxiliary variables $z_{\bar{m}}^{\Delta}{}^{(i)}$ and $\left\{y_{\bar{m},k}^{\Delta}{}^{(i)}\right\}_{k=1}^{K}$, using (27) and (29).;

3 Compute $\mathbf{p}^{(i+1)}$ by solving **P3**.;

4 Evaluate GEE: $f_{\mathrm{GEE}}{}^{(i+1)} = f_{\mathrm{GEE}}(\mathbf{p}^{(i+1)})$ in **P1**.;

5 $i \leftarrow i+1$.;

6 **end function**

B. GEE optimization via Lagrangian dual transform (LDT)

An iterative algorithm is now developed to obtain a closed-form solution for the fixed point GEE optimization problem. The Lagrangian dual transform is applied to the objective in **P1** to convert the sum of the log-ratios to the sum of ratios by moving the ratio out of the logarithm function, as shown in [53]. Therefore, the GEE maximization problem **P1** can be rewritten as

$$\textbf{P4:} \underset{\mathbf{p}, \mathbf{t}_{\bar{m}}^{\Delta}}{\mathrm{Max}} \quad \frac{\frac{\tau_d}{T}\sum_{k=1}^{K}\log_2\left(1+t_{\bar{m},k}^{\Delta}\right)}{\mathcal{P}_{\mathrm{tot}}(\mathbf{p})}, \tag{30a}$$

$$\text{s.t.} \quad t_{\bar{m},k}^{\Delta} \leq \frac{\mathrm{N}_{\bar{m},k}^{\Delta}(\mathbf{p})}{\mathrm{D}_{\bar{m},k}^{\Delta}(\mathbf{p})}, \quad \forall k, \tag{30b}$$

$$\text{(26b)}. \tag{30c}$$

Here $\left\{t_{\bar{m},1}^{\Delta}, t_{\bar{m},2}^{\Delta}, \cdots, t_{\bar{m},k}^{\Delta}\right\}$ is the set of auxiliary variables which can replace each ratio $\overline{\mathrm{SINR}}_{\bar{m},k}^{\Delta}$ inside the logarithm in **P1**. We now apply the LDT to the objective in **P4** next [53, Theorem 3] to obtain the following equivalent problem.

Theorem 3. Invoking the LDT, the problem **P4** can be recast as follows

$$\textbf{P5:} \underset{\mathbf{p}, \mathbf{t}_{\bar{m}}^{\Delta}}{\mathrm{Max}} \; f_{\mathcal{L}}(\mathbf{p}, \mathbf{t}_{\bar{m}}^{\Delta}) = \frac{1}{\mathcal{P}_{\mathrm{tot}}(\mathbf{p})} \times \frac{\tau_d}{T}\sum_{k=1}^{K}\Bigg(\underbrace{\log_2\left(1+t_{\bar{m},k}^{\Delta}\right) - \frac{t_{\bar{m},k}^{\Delta}}{\log_e(2)}}_{\mathcal{K}_1} + \underbrace{\frac{\left(1+t_{\bar{m},k}^{\Delta}\right)\mathrm{N}_{\bar{m},k}^{\Delta}(\mathbf{p})}{\log_e(2)\left(\mathrm{N}_{\bar{m},k}^{\Delta}(\mathbf{p})+\mathrm{D}_{\bar{m},k}^{\Delta}(\mathbf{p})\right)}}_{\mathcal{K}_2}\Bigg), \tag{33a}$$

$$\text{s.t.} \quad \text{(26b)}. \tag{33b}$$

Proof. The detailed proof of the above result is provided in Appendix E. □

It is observed that, for a given $\mathbf{t}_{\bar{m}}^{\Delta}$, the first term $\mathcal{K}_1$ in the numerator of $f_{\mathcal{L}}(\mathbf{p}, \mathbf{t}_{\bar{m}}^{\Delta})$ is constant, while the second term $\mathcal{K}_2$ consists of a sum of ratios. Using the results in Lemma 1, QT can now be applied by introducing the set of auxiliary variables $\left\{y_{\mathcal{Q},\bar{m},1}^{\Delta}, y_{\mathcal{Q},\bar{m},2}^{\Delta}, \cdots, y_{\mathcal{Q},\bar{m},k}^{\Delta}\right\}$ to decouple the optimization variables in $\mathcal{K}_2$. The problem **P5** can therefore be recast as follows

$$\textbf{P6:}\ \max_{\mathbf{p},\mathbf{t}^{\Delta}_{\bar{m}},\mathbf{y}^{\Delta}_{\mathcal{Q},\bar{m}}} f_{\mathcal{Q}}\big(\mathbf{p},\mathbf{t}^{\Delta}_{\bar{m}},\mathbf{y}^{\Delta}_{\mathcal{Q},\bar{m}}\big)=\frac{1}{\mathcal{P}_{\text{tot}}(\mathbf{p})}\times\frac{\tau_d}{T}\sum_{k=1}^{K}\Bigg(\log_2\big(1+t^{\Delta}_{\bar{m},k}\big)-\frac{1}{\log_e(2)}\times\big(t^{\Delta}_{\bar{m},k}-2y^{\Delta}_{\mathcal{Q},\bar{m},k}\sqrt{\big(1+t^{\Delta}_{\bar{m},k}\big)\mathrm{N}^{\Delta}_{\bar{m},k}(\mathbf{p})}+{y^{\Delta}_{\mathcal{Q},\bar{m},k}}^{2}\big(\mathrm{N}^{\Delta}_{\bar{m},k}(\mathbf{p})+\mathrm{D}^{\Delta}_{\bar{m},k}(\mathbf{p})\big)\big)\Bigg), \tag{34a}$$

$$\text{s.t.}\quad (26b), y^{\Delta}_{\mathcal{Q},\bar{m},k}\in\mathbb{R},\quad \forall k. \tag{34b}$$

It can be verified that for a given $\mathbf{p}$ and $\mathbf{t}^{\Delta}_{\bar{m}}$, the objective in **P6** is concave over $y^{\Delta}_{\mathcal{Q},\bar{m},k}$. The optimal value of $y^{\Delta}_{\mathcal{Q},\bar{m},k}$ is computed by setting $\partial f_{\mathcal{Q}}\big(\mathbf{p},\mathbf{t}^{\Delta}_{\bar{m}},\mathbf{y}^{\Delta}_{\mathcal{Q},\bar{m}}\big)/\partial \mathbf{y}^{\Delta}_{\mathcal{Q},\bar{m}}$ to zero as follows

$$y^{\Delta}_{\mathcal{Q},\bar{m},k}=\frac{\sqrt{\big(1+t^{\Delta}_{\bar{m},k}\big)\mathrm{N}^{\Delta}_{\bar{m},k}(\mathbf{p})}}{\mathrm{N}^{\Delta}_{\bar{m},k}(\mathbf{p})+\mathrm{D}^{\Delta}_{\bar{m},k}(\mathbf{p})}. \tag{35}$$

Note that **P6** is still a single-ratio non-convex optimization problem. Applying Dinkelbach's transformation [54], the problem **P6** can be recast as

$$\textbf{P7:}\ \max_{\mathbf{p},\mathbf{t}^{\Delta}_{\bar{m}},\mathbf{y}^{\Delta}_{\mathcal{Q},\bar{m}},z^{\Delta}_{\mathcal{D},\bar{m}}} f_{\mathcal{D}}\big(\mathbf{p},\mathbf{t}^{\Delta}_{\bar{m}},\mathbf{y}^{\Delta}_{\mathcal{Q},\bar{m}},z^{\Delta}_{\mathcal{D},\bar{m}}\big)=\frac{\tau_d}{T}\sum_{k=1}^{K}\Bigg(\log_2\big(1+t^{\Delta}_{\bar{m},k}\big)-\frac{1}{\log_e(2)}\times\big(t^{\Delta}_{\bar{m},k}-2y^{\Delta}_{\mathcal{Q},\bar{m},k}\sqrt{\big(1+t^{\Delta}_{\bar{m},k}\big)\mathrm{N}^{\Delta}_{\bar{m},k}(\mathbf{p})}+{y^{\Delta}_{\mathcal{Q},\bar{m},k}}^{2}\big(\mathrm{N}^{\Delta}_{\bar{m},k}(\mathbf{p})+\mathrm{D}^{\Delta}_{\bar{m},k}(\mathbf{p})\big)\big)\Bigg)-z^{\Delta}_{\mathcal{D},\bar{m}}\big(\mathcal{P}_{\text{tot}}(\mathbf{p})\big), \tag{36a}$$

$$\text{s.t.}\quad (26b), y^{\Delta}_{\mathcal{Q},\bar{m},k}\in\mathbb{R}, z^{\Delta}_{\mathcal{D},\bar{m}}\in\mathbb{R}. \tag{36b}$$

It can be verified from (36) that the objective in **P7** is linear over $(\mathbf{p}, z^{\Delta}_{\mathcal{D},\bar{m}})$ and quadratic over $\mathbf{y}^{\Delta}_{\mathcal{Q},\bar{m}}$, where $z^{\Delta}_{\mathcal{D},\bar{m}}$ is an auxiliary variable used for decoupling the numerator and denominator in **P6**. Therefore, the optimal value of $z^{\Delta}_{\mathcal{D},\bar{m}}$ for a given $\big(\mathbf{p},\mathbf{y}^{\Delta}_{\mathcal{Q},\bar{m}}\big)$ is updated iteratively as

$$z^{\Delta}_{\mathcal{D},\bar{m}}=\frac{1}{\mathcal{P}_{\text{tot}}(\mathbf{p})}\times\frac{\tau_d}{T}\sum_{k=1}^{K}\Bigg(\log_2\big(1+t^{\Delta}_{\bar{m},k}\big)-\frac{1}{\log_e(2)}\big(t^{\Delta}_{\bar{m},k}-2y^{\Delta}_{\mathcal{Q},\bar{m},k}\sqrt{\big(1+t^{\Delta}_{\bar{m},k}\big)\mathrm{N}^{\Delta}_{\bar{m},k}(\mathbf{p})}+{y^{\Delta}_{\mathcal{Q},\bar{m},k}}^{2}\big(\mathrm{N}^{\Delta}_{\bar{m},k}(\mathbf{p})+\mathrm{D}^{\Delta}_{\bar{m},k}(\mathbf{p})\big)\big)\Bigg). \tag{37}$$

It is observed that for a given $(z^{\Delta}_{\mathcal{D},\bar{m}},\mathbf{y}^{\Delta}_{\mathcal{Q},\bar{m}})$, the objective in **P7** is concave over $\mathbf{p}$, since as can be seen from (20) and (23) respectively, $\mathrm{N}^{\Delta}_{\bar{m},k}(\mathbf{p})$ and $\mathrm{D}^{\Delta}_{\bar{m},k}(\mathbf{p})$, are affine functions of $\mathbf{p}$. Therefore, the closed-form update equations of the optimal user transmit powers are obtained by setting $\partial f_{\mathcal{D}}\left(\mathbf{p},\mathbf{t}^{\Delta}_{\bar{m}},\mathbf{y}^{\Delta}_{\mathcal{Q},\bar{m}},z^{\Delta}_{\mathcal{D},\bar{m}}\right)/\partial p_{\bar{m},k}$ to zero as shown in (31) and (32) (shown at the bottom of this page).

To summarize, GEE optimization using the LDT framework is carried out by sequentially following the steps below: i) Lagrangian dual transform [53]; ii) Quadratic transform [51]; and iii) Dinkelbach's transform [54] to transform **P1** into **P7** and iteratively update the power variables. The step-by-step procedure of EMF-aware GEE optimization via LDT is succinctly described in Algorithm 2, which computes $\{t^{\Delta}_{\bar{m},k}\}^{K}_{k=1}$ in Step 2; auxiliary variables $\left\{y^{\Delta}_{\mathcal{Q},\bar{m},k}\right\}^{K}_{k=1}$ and $z^{\Delta}_{\mathcal{D},\bar{m}}$ in Step 3; and the optimal transmit power $\mathbf{p}$ in Step 5.

Algorithm 2: EMF aware GEE maximization using the LDT

Input: Given a tolerance $\epsilon>0$, SAR thresholds $\{q_k\}^{K}_{k=1}$ and reference SAR values $\{SAR_{ref}\}^{K}_{k=1}$. Initialize $\left\{P_k\right\}^{K}_{k=1}$ with equal power allocation i.e., $\left\{P_k{}^{(0)}\right\}^{K}_{k=1}=\frac{P^{\max}_k}{K}$. Initialize $f_{\text{GEE}}{}^{(0)}=f_{\text{GEE}}\big(\mathbf{p}^{(0)}\big)$. Set $i=0$.

Output: $\mathbf{p}^{*}=\left\{P_k{}^{*}\right\}^{K}_{k=1}$ as the solutions.

1 **while** $\|f_{\text{GEE}}{}^{(i+1)}-f_{\text{GEE}}{}^{(i)}\|>\epsilon$

2 Given a feasible $\mathbf{p}^{(i)}$, compute the auxiliary variables $\{t^{\Delta}_{\bar{m},k}{}^{(i)}\}^{K}_{k=1}$ from (30b).;

3 Compute auxiliary variable $\left\{y^{\Delta}_{\mathcal{Q},\bar{m},k}{}^{(i)}\right\}^{K}_{k=1}$ and $z^{\Delta}_{\mathcal{D},\bar{m}}{}^{(i)}$, using (35) and (37).;

4 Compute $t^{\Delta}_{\bar{m},k}{}^{*(i)}$ using (61) in Appendix C.;

5 Compute $\mathbf{p}^{(i+1)}$, using (31) and (32).;

6 Evaluate GEE: $f_{\text{GEE}}{}^{(i+1)}=f_{\text{GEE}}\big(\mathbf{p}^{(i+1)}\big)$ in **P1**.;

7 $i\leftarrow i+1$.;

8 **end function**

C. Computational Complexity of the proposed algorithms:

- *Complexity of Algorithm 1:* The overall complexity of Algorithm 1 is calculated by quantifying the complexity of the auxiliary variables $\left(z^{\Delta}_{\bar{m}},\{y^{\Delta}_{\bar{m},k}\}^{K}_{k=1}\right)$ in Step-2 and solving **P3** in Step-3.
  - The calculation of $z^{\Delta}_{\bar{m}}$ in (27) requires K real additions once the $\overline{\text{SINR}}^{\Delta}_{\bar{m},k}$ value is obtained. The complexity of calculating $\overline{\text{SINR}}^{\text{MRC}}_{\bar{m},k}$ is determined by its closed from expression in Appendix C, which is dominated by the expression in (54) and it is on the order of $\mathcal{O}(K)$. Similarly, the complexity of calculating $\overline{\text{SINR}}^{\text{ZF}}_{\bar{m},k}$ in (16) is determined in Appendix D, which is equal to $\mathcal{O}(K)$ as it is dominated by the expression in (60). Thus, the overall complexity of computing $z^{\Delta}_{\bar{m}}$ is $\mathcal{O}(K^2)$ for both the MRC and ZF techniques.
  - Similarly, computing $y^{\Delta}_{\bar{m},k}$ requires the calculation of the terms $N^{\Delta}_{\bar{m},k}(\mathbf{p})$ and $D^{\Delta}_{\bar{m},k}(\mathbf{p})$ having complexities of $\mathcal{O}(1)$ and $\mathcal{O}(K)$ respectively, for both the MRC and ZF receivers. Thus, the complexity of computing

$$P^{\text{MRC}*}_{k}=\min\left\{\frac{q_k}{SAR_{ref}},P^{\max}_{k},\frac{NP_p\beta^2_k{y^{\Delta}_{\mathcal{Q},\bar{m},k}}^{2}\big(t^{\Delta}_{\bar{m},k}+1\big)}{\big(\frac{\tau_d}{T}z^{\Delta}_{\mathcal{D},\bar{m}}\upsilon^{-1}_{U}\log_e(2)+{y^{\Delta}_{\mathcal{Q},\bar{m},k}}^{2}\big((N+1)P_p\beta^2_k+\beta_k\sigma^2_\eta\big)\big)^2}\right\},\ \text{and} \tag{31}$$

$$P^{\text{ZF}*}_{k}=\min\left\{\frac{q_k}{SAR_{ref}},P^{\max}_{k},\frac{(N-K)P_p\beta^2_k{y^{\Delta}_{\mathcal{Q},\bar{m},k}}^{2}\big(t^{\Delta}_{\bar{m},k}+1\big)}{\big(\frac{\tau_d}{T}z^{\Delta}_{\mathcal{D},\bar{m}}\upsilon^{-1}_{U}\log_e(2)+{y^{\Delta}_{\mathcal{Q},\bar{m},k}}^{2}\big((N-K)P_p\beta^2_k+\beta_k\sigma^2_\eta\big)\big)^2}\right\}. \tag{32}$$

Table II: System Parameters.

Parameter	Specification	Parameter	Specification
Noise variance , σ_η^2	-94 dBm	Shadow fading, σ_z^2	10 dB
Number of users, K	8	Path loss Exponent, ν	3.76
Number of BS antenna, N	128	Reference SAR, $\{SAR_{ref}\}_{k=1}^K$	0.0047 W/kg
Number of subcarriers, M	256	Channel coherence time, T_c	1ms = 196 symbols (1ms / 66.7μs)
Constellation	4-QAM	Number of channel taps, L	3 with uniform power delay profile
Subcarrier spacing	15kHz	Training symbols per subcarrier	K
Symbol duration, T	66.7μs	Prototype filter	Isotropic orthogonal transform algorithm (IOTA) with duration $4T$

$y_{\bar{m},k}^{\Delta}$ is $\mathcal{O}(K)$, and therefore the overall complexity of computing $\{y_{\bar{m},k}^{\Delta}\}_{k=1}^K$ is $\mathcal{O}(K^2)$.

– The interior-point method is used for solving the convex problem **P3**, resulting in a complexity order of $\mathcal{O}\big[(K)^{3.5}\big]$.

Thus, Algorithm 1 solves the GEE maximization problem involving $2K+1$ real variables and $2K$ constraints which has the overall computational complexity order of $\mathcal{O}\left[\mu_\pi\left((K)^{3.5}+2K^2\right)\right]$, where μ_π is the number of iterations required for the convergence of Algorithm 1.

- *Complexity of Algorithm 2:* This computes the auxiliary variables $\left(\{t_{\bar{m},k}^{\Delta}\}_{k=1}^K, \left\{y_{\mathcal{Q},\bar{m},k}^{\Delta}\right\}_{k=1}^K, z_{\mathcal{D},\bar{m}}^{\Delta}\right)$ in Step-2 and Step-3, and the power variables $\left(\{P_k^{\text{MRC}}\}_{k=1}^K, \{P_k^{\text{ZF}}\}_{k=1}^K\right)$ over each iteration using the update equations (61), (35), (37), (31), and (32).

  – The computational complexity of $t_{\bar{m},k}^{\Delta} = \frac{\text{N}_{\bar{m},k}^{\Delta}(\mathbf{p})}{\text{D}_{\bar{m},k}^{\Delta}(\mathbf{p})}$ in (61) is determined by the number of operations required for calculating $\text{N}_{\bar{m},k}^{\Delta}(\mathbf{p})$ and $\text{D}_{\bar{m},k}^{\Delta}(\mathbf{p})$ which are of order $\mathcal{O}(1)$ and $\mathcal{O}(K)$, respectively. Therefore, the complexity of evaluating ${t_{\bar{m},k}^{\Delta}}^*$ is $\mathcal{O}(K)$.

  – The complexity of computing the auxiliary variable $y_{\mathcal{Q},\bar{m},k}^{\Delta}$ in (35) that requires the calculation of $t_{\bar{m},k}^{\Delta}$, $\text{N}_{\bar{m},k}^{\Delta}(\mathbf{p})$ an $\text{D}_{\bar{m},k}^{\Delta}(\mathbf{p})$ is equal to $\mathcal{O}(K)$.

  – Similarly, the computation of the auxiliary variable $z_{\mathcal{D},\bar{m}}^{\Delta}$ in (37) requires the calculation of $t_{\bar{m},k}^{\Delta}$, $\text{N}_{\bar{m},k}^{\Delta}(\mathbf{p})$ and $\text{D}_{\bar{m},k}^{\Delta}(\mathbf{p})$. Furthermore, it also requires K real additions, and has an overall complexity of $\mathcal{O}(K^2)$.

  – It is observed from the $P_k^{\text{MRC}^*}$ and $P_k^{\text{ZF}^*}$ expressions in (31), and (32) that an identical number of operations is required to derive the optimal power variables for both the MRC and ZF receivers, respectively. The computational complexity of evaluating $P_k^{\Delta^*}$ for $\Delta = \{\text{MRC, ZF}\}$, is dominated mainly by the calculation of $z_{\mathcal{D},\bar{m}}^{\Delta}$ and equals $\mathcal{O}(K^2)$.

  Thus, the overall complexity of Algorithm 2 is $\mathcal{O}\left[\kappa_\pi\left(2K+2K^2\right)\right]$. The term κ_π denotes the number of iterations required for Algorithm 1 to converge.

It is important to note here that the complexity of Algorithm 2 is extremely low in comparison to that of Algorithm 1. This is therefore well-suited for GEE maximization in real-world systems.

V. Simulation results

This section presents the results of a simulation study to validate the various analytical expressions derived for the FBMC-based massive MIMO systems and also to illustrate the performance of the proposed techniques. The effectiveness of the GEE optimization algorithm and the effect of the EM exposure index (EI) on the GEE performance is also studied. The users are considered to be located uniformly at random within a disc around the BS. The users are placed at distances d_k in the range $35m \leq d \leq 1000m$ from the BS. The large-scale fading parameters for the kth user is modelled as $\beta_k[\text{dB}] = -37.3 - 10\nu\log_{10}\left(\frac{d_k}{1\text{m}}\right) + z_k$, where ν is the path-loss exponent and z_k denotes the shadow fading factor having the pdf of $\mathcal{N}(0,\sigma_z^2)$. The large-scale fading parameters are normalized relative to the noise variance σ_η^2 [44]. The parameters of circuit power consumption P_{FIX}, P_{BS} and P_{UE} are set as 10 W, 0.4 W and 0.2 W, respectively. The remaining components of the power consumption model are set as given in [44, ch. 5, Table 5.3]. The MMSE estimator based on the IAM framework is utilized for channel estimation. The number of zeros between adjacent training symbols in the preamble is set as $z = 3$. The other simulation parameters are given in Table II, unless stated otherwise.

A. Validation of the SE lower-bounds

The closed-form expressions of the uplink sum-rate derived in Theorem 1 and 2 are validated in this subsection by comparing them to their respective ergodic SE expressions in (13) and (15). Equal power allocation (EPA) is used among the users, i.e., $P_{\text{max}} = \frac{P_T}{K}$ with P_{max} being the maximum allowed transmit power of each user. Fig. 2a demonstrates the uplink sum-rate versus transmit power P_T performance for different number of BS antennas. It is observed that the simplified closed-form expressions of both the MRC and ZF receivers closely follow their respective ergodic SE plots. This clearly validates the accuracy of the closed-form lower-bounds derived for both the MRC and ZF receivers. Since the ZF receiver mitigates the MUI, it outperform the MRC receiver in the high-power regime.

B. Impact of pilot pattern on SE performance analysis

Recall that the MMSE estimator of Section II-B is based on the IAM framework. Many pilot patterns have been described in the FBMC literature for the IAM framework to improve the quality of channel estimates [8]. Fig. 2b shows the impact of two popular pilot patterns, namely the IAM and IAM-complex (IAMC) on the SE of the ZF and MRC receivers. It is observed that the SE achieved using the IAMC training structure is higher than that of its IAM counterpart for both the MRC and ZF receivers. This is due to the fact that the power of the virtual training symbols at the receiver is higher for the IAMC training sequence than that of the IAM sequence [8]. A

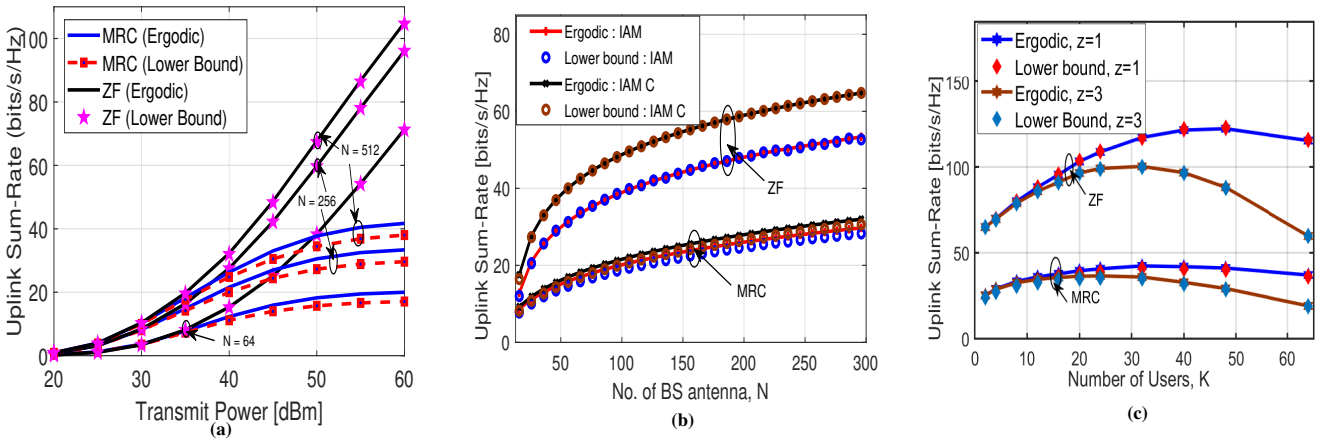

Fig. 2: (a) Uplink sum rate vs transmit power P_T for a given number of BS antennas with number of users $K = 12$; (b) Uplink sum rate vs the number of BS antenna N for IAM and IAMC channel estimation with $P_T = 55$ dBm and $K = 12$; (c) Uplink sum rate vs the number of users K for a given number of zeros z used for channel estimation with $P_T = 55$ dBm.

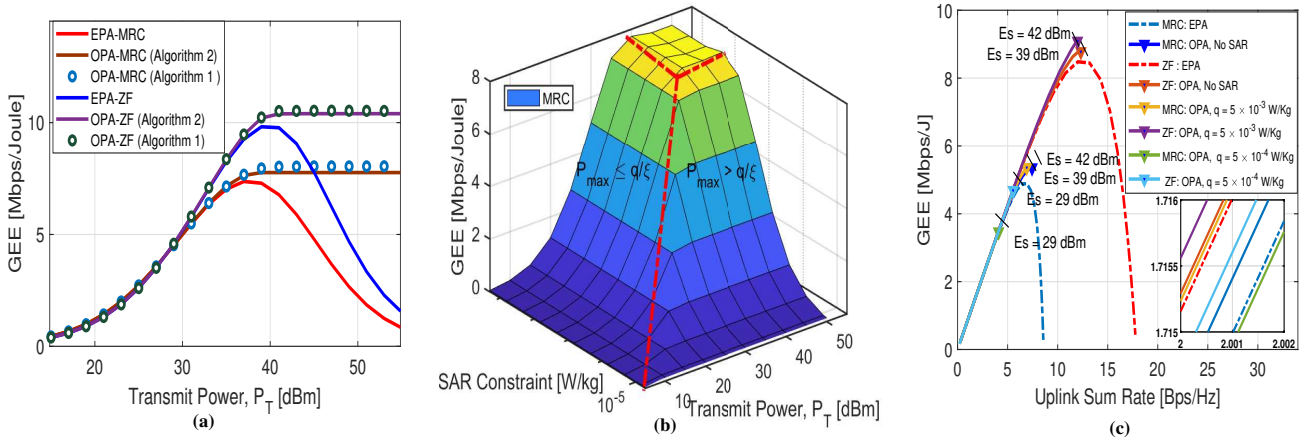

Fig. 3: (a) GEE vs transmit power P_T with $K = 4$ users and $N = 64$ BS antennas; (b) GEE as function of Transmit power P_T and SAR constraint q; (c) GEE - SE trade off for $P_T = [15 : 2 : 55]$ dBm, user pairs $K = 4$ and BS antenna $N = 64$.

trend similar to that of Fig. 2a has been observed here also for both the IAM and IAMC based channel estimation schemes, wherein the closed-form SE expressions serve as lower-bounds for the achievable SE. The plots in Fig. 2c compare the SE versus the number of users K for different values of the number of zeros z inserted between the adjacent pilot symbols to estimate the channel using the FBMC frame structure of Fig. 1. For this study, the total transmit power of $P_T = 55$ dBm is divided equally among the users and number of BS antennas which is $N = 128$. It can be seen that the analytical plots corresponding to the closed-form SE expressions closely match with the ergodic SE values for both the MRC and ZF receivers. As expected, the SE decreases with an increase in the number of zeros, because the latter increases the pilot overhead required for channel estimation, as also shown in the frame structure of Fig. 1. For a large number of users $(K > 50)$, it is noticed that the rate of decrease in the SE of the ZF receiver is higher than that of the MRC receiver. This is because the transmit power per user decreases with an increase in the value of K. Due to this the noise power starts dominating the MUI power. As a result, maximizing the SNR is more effective than suppressing the MUI. This leads to a sharp decrease in the SE of the ZF receiver in comparison to its MRC counterpart.

C. GEE optimization

Fig. 3a plots the GEE versus transmit power P_T for the MRC and ZF receivers by choosing $K = 4$ and $N = 64$. For this study, the user transmit power constraints in (25b) are considered without any SAR constraints. The impact of the SAR constraint is investigated in Fig. 3b. It is observed that for $P_T \leq 40$ dBm, the GEE obtained using the EPA increases with P_T, whereas for $P_T > 40$ dBm, the denominator in (24) starts to dominate, which leads to a decrease in the GEE. The GEE obtained using the proposed algorithms for both the MRC and ZF receivers first increases with the transmit power for $P_T < 40$ dBm and saturates for $P_T > 40$ dBm. It is also observed that the GEE obtained using Algorithm 1 closely matches the GEE attained using Algorithm 2.

D. Impact of SAR constraints on GEE optimization

Fig. 3b plots the GEE by varying the transmit power and SAR thresholds. For this study, MRC combining is considered at the BS. The SAR threshold is set to be equal for all the users, i.e., $\{q_k\}_{k=1}^{K} = q$. The GEE obtained in Fig. 3b can be divided into two regimes i) the low transmit power regime: $P_{\max} \leq \frac{q}{\xi}$ and ii) the high transmit power regime: $P_{\max} > \frac{q}{\xi}$. It can be seen that in the low transmit power regime, the GEE

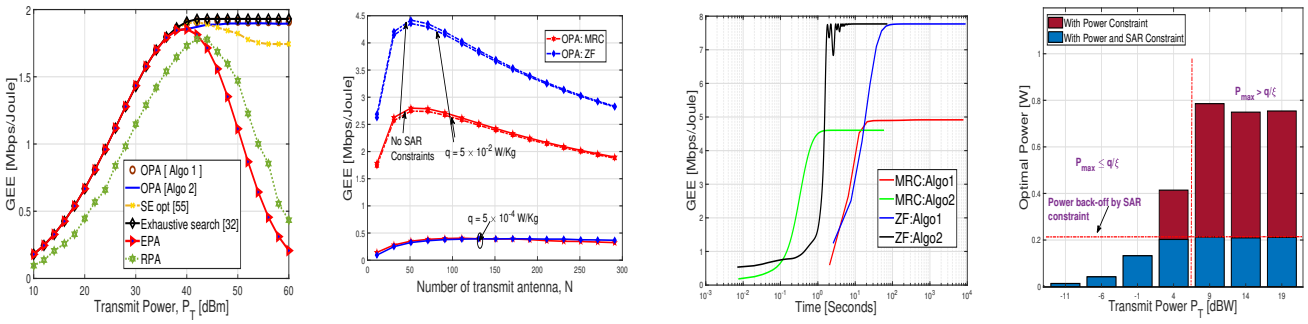

Fig. 4: (a) Comparison of proposed GEE optimization algorithms with others state-of-art approaches with $K = 2$, $N = 128$ and SAR threshold, $q_k = 0.05$ W/kg, $\forall k$; (b) GEE vs number of BS antennas N for transmit power $P_T = 40$ dBm and user pairs $K = 4$; (c) GEE vs run time for transmit power $P_T = 55$ dBm, BS antenna $N = 50$, and user pairs $K = 4$; (d) Optimal power allocation for UE having stronger large scale fading channel coefficient (β) with and without SAR constraint.

performance is restricted by the transmit power constraint only. By contrast, in the high transmit power regime, the GEE first increases with q and then saturates. It is worth noting that, for $q \geq 2 \times 10^{-2}$ W/kg, $P_T \geq 40$ dBm, the GEE becomes invariant to the choice of P_T as well as q and attains a constant value. These observations inform the system designer about the minimum SAR threshold and transmit power required for maximizing the GEE. It is also inferred from Fig. 3b that the GEE performance is not negatively impacted by the SAR limit of 0.08 W/kg specified by the international regulation (ICNIRP) to avoid any potential deleterious impact that can arise due to EM exposure [35]. Similar observations can be made for the ZF receiver.

E. Impact of SAR constraints on the GEE versus SE trade-off

Fig. 3c plots the GEE versus SE by varying the transmit power P_T from 15 dBm to 55 dBm. For this study, the values of the SAR threshold are set as $q \in \{1\text{W/kg}, 5 \times 10^{-3}\text{W/kg}, 5 \times 10^{-4}\text{W/kg}\}$ [35]. These values correspond to negligible, relaxed and tight SAR constraints, respectively. The GEE obtained with OPA by using the proposed algorithms is also compared to its EPA counterpart for both the MRC and ZF receivers. For $P_T \leq 39$ dBm in case of the MRC receiver and $P_T \leq 42$ dBm in case of the ZF receiver, both the GEE with EPA and the SE monotonically increase with P_T. After that, the SE keeps improving with P_T at the cost of a drop in the GEE. Moreover, it is worth noting that for the OPA scheme, the GEE versus SE curve monotonically increases by varying P_T and reaches its peak for both the MRC and the ZF receivers at $P_T = 39$ dBm and $P_T = 42$ dBm, respectively. This is because the optimal transmit power stops increasing once the GEE saturates to a finite value. It can also be observed that as the SAR threshold decreases, the GEE versus SE curve reaches its maximum value at lower transmit power. This is because the optimal transmit power required to satisfy the tight SAR constraint is lower, which in turn leads to a degradation of both the GEE and SE.

Fig. 4a characterizes the performance of the proposed GEE optimization Algorithms 1 and 2 by comparing them with the i) exhaustive search approach [32], which obtains the global optimal solution by exhaustively searching over the entire variable space; ii) existing SE optimization in [55], which allocates the power to optimize the network SE; iii) EPA scheme and iv) random power allocation (RPA), where the users are allocated random power values. This study is performed by setting $N = 128$, and $K = 2$ for the MRC receiver and the same setup can also be easily applied to the ZF receiver. The SAR threshold for each user is set as $q = 0.05$ W/kg which is strictly lower than the limits set by the ICNIRP (i.e. 0.08 W/kg). It is first discovered that the performance of the GEE obtained using the proposed optimization algorithms is approximately equal to that of the global optimal solution obtained by the exhaustive search technique, therefore, validating the effectiveness of the proposed algorithm. Note that the complexity order of the exhaustive search scheme is $\mathcal{O}(N^K)$, which is significantly higher than that the proposed algorithms and grows exponentially with the number of users. Next, it is observed that the GEE obtained using the proposed optimization frameworks is superior to the GEE obtained using the SE optimization technique of [55]. This is because the SE optimization scheme maximizes the network SE by allocating a significant proportion of the available power, but the GEE maximization approach curtails allocating additional power once the GEE is maximized. As a result, the GEE obtained using SE optimization begins to decrease after attaining its peak. As a result, the GEE saturates at a high transmit power. It is also observed that the RPA schemes follow trends similar to those of the EPA scheme.

Fig. 4b plots the GEE versus the number of BS antennas N for both the MRC and ZF receivers at the SAR thresholds $q \in \{1\text{W/kg}, 5 \times 10^{-2}\text{W/kg}, 5 \times 10^{-4}\text{W/kg}\}$ and the transmit power $P_T = 40$ dBm. It is observed that when no SAR constraint is imposed, the GEE increases with N, for $N \leq 60$, and $N \leq 50$ corresponding to the ZF, and MRC receivers, respectively. This is because in this regime, the increase in SE dominates the related increase in the network's power consumption. Subsequently, for $N > 60$ and $N > 50$, the GEE starts decreasing with N for the ZF and MRC, respectively. This can be attributed to the fact that the increase in SE for this range of values of the parameter N is not significant enough to compensate for the increased network power consumption.

F. Convergence analysis

Fig. 4c investigates the convergence of the proposed NQT-based and LDT-based algorithms. The convergence of Algo-

rithms 1 and 2 with respect to the CPU time for both the MRC and ZF receivers are presented by considering $K = 4$, $N = 50$, and $P_T = 55$ dBm. The convergence threshold for both the algorithms is set as $\epsilon = 10^{-6}$. It is observed that Algorithm 1 requires 60 seconds to converge to a stationary point, while Algorithm 2 requires roughly 1 second for convergence. This is because Algorithm 2 has a significantly lower cost per iteration than Algorithm 1 due to closed-form updates over each iteration, whereas Algorithm 1 has to solve a convex problem over each iteration. The respective computational complexities of both the algorithms have been explicitly evaluated in Sections IV-A and IV-B.

G. Impact of SAR constraints on the power allocation policy

Fig. 4d investigates the impact of SAR constraints by plotting the transmit power via the optimal power allocation (on y-axis) and equal power allocation (on x-axis) schemes with the MRC receiver. This study is focused on the optimal power allocation of the user that experiences the strongest large-scale coefficient β. This is owing to the fact that when the power allocated to a user with the strongest β satisfies both the transmit power and SAR constraints, the power allocated to all the other users also satisfies both the constraints. The bar plot clearly shows the effect of employing only power constraints on the optimal power allocation vis-à-vis employing both the transmit power and SAR constraints. It can be seen that for $P_T < 0$ dBW, the SAR constraints do not impact the optimal power allocation due to the fairly small transmit power that is potentially harmless for the human body. Therefore, the GEE algorithm exploits the full power budget, which leads to the bar plots overlapping completely with each other. In this regime, the optimal power is controlled only by the power constraints. On the other hand, for $P_T > 0$ dBW, a significant drop is recorded in the optimal power, which has to be reduced from its maximum possible value to avoid any harmful effects of EM exposure. Therefore, the power constraints are slack and the optimal power is controlled by the SAR constraints only. This is termed the power back-off regime in the context of EMF-aware cellular networks [33].

VI. Conclusion

The SE and EE of the FBMC based multi-user massive MIMO uplink systems has analyzed considering also the health concerns associated with EMF exposure. Closed-form lower-bound expressions were derived for the uplink spectral efficiency for both the MRC and ZF receivers relying on imperfect CSI. Furthermore, the asymptotic SE performance was also investigated for large values of the transmit power. Two novel algorithms based on the NQT and LDT frameworks were proposed for optimizing the non-convex GEE metric under power and SAR constraints. Our numerical results validated the various SE expressions developed and also demonstrated the enhanced GEE performance of the proposed optimization approaches. Finally, it was also seen that a higher GEE can be achieved while meeting the users EMF exposure constraints using the algorithms presented, which paves the way for their safe deployment in next-generation networks.

Appendix A

Upon replacing $\mathbf{w}_{\bar{m}}^k$ by $\widehat{\mathbf{g}}_{\bar{m}}^k$ in (9), the power of the each term of the quantity $d_{\bar{m},\bar{n}}^k$ can be simplified as

$$\mathbb{E}\big[\big(\widehat{d}_{\bar{m},\bar{n}}^k\big)^2\big] = \mathbb{E}\big[\big(\Re\left\{\|\widehat{\mathbf{g}}_{\bar{m}}^k\|^2 b_{\bar{m},\bar{n}}^k\right\}\big)^2\big] + \mathrm{Var}\big[\vartheta_{\bar{m},\bar{n}}^{k,\mathrm{MRC}}\big], \tag{38}$$

where the first term in (38) is the desired signal term that can be simplified as $\mathbb{E}\big[\big(\Re\left\{\|\widehat{\mathbf{g}}_{\bar{m}}^k\|^2 b_{\bar{m},\bar{n}}^k\right\}\big)^2\big] = \|\widehat{\mathbf{g}}_{\bar{m}}^k\|^2 \mathbb{E}\big[\big(\Re\left\{b_{\bar{m},\bar{n}}^k\right\}\big)^2\big] = P_k \|\widehat{\mathbf{g}}_{\bar{m}}^k\|^2$.

The second term in (38) denotes the variance of the interference-plus-noise $\vartheta_{\bar{m},\bar{n}}^{k,\mathrm{MRC}}$ that can be expressed as

$$\begin{aligned}\mathrm{Var}\big[\vartheta_{\bar{m},\bar{n}}^{k,\mathrm{MRC}}\big] =& \mathbb{E}\big[\big(\Re\big\{\sum_{\substack{j=1\\ j\neq k}}^{K}\big(\widehat{\mathbf{g}}_{\bar{m}}^k\big)^H \widehat{\mathbf{g}}_{\bar{m}}^j b_{\bar{m},\bar{n}}^j + \sum_{j=1}^{K}\big(\widehat{\mathbf{g}}_{\bar{m}}^k\big)^H \mathbf{e}_{\bar{m}}^j b_{\bar{m},\bar{n}}^j \\ &+ \big(\widehat{\mathbf{g}}_{\bar{m}}^k\big)^H \boldsymbol{\eta}_{\bar{m},\bar{n}}\big\}\big)^2\big], \end{aligned} \tag{39}$$

$$\begin{aligned}\mathrm{Var}\big[\vartheta_{\bar{m},\bar{n}}^{k,\mathrm{MRC}}\big] \overset{(a)}{=}& \mathbb{E}\big[\big(\Re\big\{\sum_{\substack{j=1\\ j\neq k}}^{K}\big(\widehat{\mathbf{g}}_{\bar{m}}^k\big)^H \widehat{\mathbf{g}}_{\bar{m}}^j b_{\bar{m},\bar{n}}^j\big\}\big)^2\big] \\ &+ \mathbb{E}\big[\big(\Re\big\{\sum_{j=1}^{K}\big(\widehat{\mathbf{g}}_{\bar{m}}^k\big)^H \mathbf{e}_{\bar{m}}^j b_{\bar{m},\bar{n}}^j\big\}\big)^2\big] \\ &+ \mathbb{E}\big[\big(\Re\big\{\big(\widehat{\mathbf{g}}_{\bar{m}}^k\big)^H \boldsymbol{\eta}_{\bar{m},\bar{n}}\big\}\big)^2\big]. \end{aligned} \tag{40}$$

The equality in (a) holds because the terms in (39) are independent. The power of the first term above can be simplified as

$$\begin{aligned}&\mathbb{E}\big[\big(\Re\big\{\sum_{\substack{j=1\\ j\neq k}}^{K}\big(\widehat{\mathbf{g}}_{\bar{m}}^k\big)^H \widehat{\mathbf{g}}_{\bar{m}}^j b_{\bar{m},\bar{n}}^j\big\}\big)^2\big] \\ &= \mathbb{E}\big[\big(\sum_{\substack{j=1\\ j\neq k}}^{K}\big(\Re\big\{\big(\widehat{\mathbf{g}}_{\bar{m}}^k\big)^H \widehat{\mathbf{g}}_{\bar{m}}^j\big\}\Re\big\{b_{\bar{m},\bar{n}}^j\big\} - \Im\big\{\big(\widehat{\mathbf{g}}_{\bar{m}}^k\big)^H \widehat{\mathbf{g}}_{\bar{m}}^j\big\}\Im\big\{b_{\bar{m},\bar{n}}^j\big\}\big)\big)^2\big] \\ &\overset{(a)}{=} \sum_{\substack{j=1\\ j\neq k}}^{K}\Big(\big(\Re\big\{\big(\widehat{\mathbf{g}}_{\bar{m}}^k\big)^H \widehat{\mathbf{g}}_{\bar{m}}^j\big\}\big)^2 \mathbb{E}\big[\big(\Re\big\{b_{\bar{m},\bar{n}}^j\big\}\big)^2\big] \\ &\quad + \big(\Im\big\{\big(\widehat{\mathbf{g}}_{\bar{m}}^k\big)^H \widehat{\mathbf{g}}_{\bar{m}}^j\big\}\big)^2 \mathbb{E}\big[\big(\Im\big\{b_{\bar{m},\bar{n}}^j\big\}\big)^2\big]\Big) \\ &\overset{(b)}{=} \sum_{\substack{j=1\\ j\neq k}}^{K} P_j\Big(\big(\Re\big\{\big(\widehat{\mathbf{g}}_{\bar{m}}^k\big)^H \widehat{\mathbf{g}}_{\bar{m}}^j\big\}\big)^2 + \big(\Im\big\{\big(\widehat{\mathbf{g}}_{\bar{m}}^k\big)^H \widehat{\mathbf{g}}_{\bar{m}}^j\big\}\big)^2\Big) \\ &= \sum_{\substack{j=1\\ j\neq k}}^{K} P_j\big|\big(\widehat{\mathbf{g}}_{\bar{m}}^k\big)^H \widehat{\mathbf{g}}_{\bar{m}}^j\big|^2. \end{aligned} \tag{41}$$

The equality (a) is obtained by considering i) $\mathbf{E}\big[\Re\{b_{\bar{m},\bar{n}}^i\}\Im\{b_{\bar{m},\bar{n}}^i\}\big] = 0$; ii) $\mathbf{E}\big[\Re\{b_{\bar{m},\bar{n}}^i\}\Re\{b_{\bar{m},\bar{n}}^j\}\big] = 0$; and iii) $\mathbf{E}\big[\Im\{b_{\bar{m},\bar{n}}^i\}\Im\{b_{\bar{m},\bar{n}}^j\}\big] = 0$. Equality (b) refers to the fact that the power of the intrinsic interference is approximately equal to the OQAM symbol power, i.e. $\mathbb{E}\big[|I_{\bar{m},\bar{n}}^k|^2\big] \approx P_k$. Therefore, one can write $\mathbb{E}\big[\big(\Im\big\{b_{\bar{m},\bar{n}}^j\big\}\big)^2\big] \approx \mathbb{E}\big[\big(\Re\big\{b_{\bar{m},\bar{n}}^j\big\}\big)^2\big]$. Along similar lines, one can simplify the variance of the remaining terms of $\vartheta_{\bar{m},\bar{n}}^{k,\mathrm{MRC}}$. Thus, the final expression for the

variance of the quantity $\vartheta_{\bar{m},\bar{n}}^{k,\text{MRC}}$ can be written as

$$\text{Var}\left[\vartheta_{\bar{m},\bar{n}}^{k,\text{MRC}}\right] = \sum_{\substack{j=1\\ j\neq k}}^{K} P_j \left|\left(\widehat{\mathbf{g}}_{\bar{m}}^{k}\right)^H \widehat{\mathbf{g}}_{\bar{m}}^{j}\right|^2 + \sum_{j=1}^{K} P_j \left|\left(\widehat{\mathbf{g}}_{\bar{m}}^{k}\right)^H \mathbf{e}_{\bar{m}}^{j}\right|^2 + \|\widehat{\mathbf{g}}_{\bar{m}}^{k}\|^2 \frac{\sigma_\eta^2}{2}. \tag{42}$$

APPENDIX B

The covariance matrix of the effective noise $\boldsymbol{\vartheta}_{\bar{m},\bar{n}}^{\text{ZF}}$ can be simplified as

$$\begin{aligned}\text{Cov}\left[\boldsymbol{\vartheta}_{\bar{m},\bar{n}}^{\text{ZF}}\right] &= \mathbb{E}\left[\boldsymbol{\vartheta}_{\bar{m},\bar{n}}^{\text{ZF}} (\boldsymbol{\vartheta}_{\bar{m},\bar{n}}^{\text{ZF}})^H\right] \\ &= \text{Cov}\left[\Re\{\widehat{\mathbf{G}}_{\bar{m}}^{\dagger} \mathbf{E}_{\bar{m}} \mathbf{b}_{\bar{m},\bar{n}}\}\right] + \text{Cov}\left[\Re\{\widehat{\mathbf{G}}_{\bar{m}}^{\dagger} \boldsymbol{\eta}_{\bar{m},\bar{n}}\}\right].\end{aligned} \tag{43}$$

The second term of the covariance of $\boldsymbol{\vartheta}_{\bar{m},\bar{n}}^{k,\text{ZF}}$ in (43) can be simplified as

$$\begin{aligned}&\text{Cov}\left[\Re\{\widehat{\mathbf{G}}_{\bar{m}}^{\dagger} \boldsymbol{\eta}_{\bar{m},\bar{n}}\}\right] \\ &= \text{Cov}\left[\Re\{(\widehat{\mathbf{G}}_{\bar{m}}^H \widehat{\mathbf{G}}_{\bar{m}})^{-1} \widehat{\mathbf{G}}_{\bar{m}}^H \boldsymbol{\eta}_{\bar{m},\bar{n}}\}\right] \\ &= \text{Cov}\left[\Re\{(\widehat{\mathbf{G}}_{\bar{m}}^H \widehat{\mathbf{G}}_{\bar{m}})^{-1} \left[(\widehat{\mathbf{g}}_{\bar{m}}^1)^H \boldsymbol{\eta}_{\bar{m},\bar{n}}, (\widehat{\mathbf{g}}_{\bar{m}}^2)^H \boldsymbol{\eta}_{\bar{m},\bar{n}}, \cdots, (\widehat{\mathbf{g}}_{\bar{m}}^K)^H \boldsymbol{\eta}_{\bar{m},\bar{n}}\right]^T\}\right]. \\ &= \begin{bmatrix} \mathbb{E}\left[\left(\Re\{\left[(\widehat{\mathbf{G}}_{\bar{m}}^H \widehat{\mathbf{G}}_{\bar{m}})^{-1}\right]_{1,1} (\widehat{\mathbf{g}}_{\bar{m}}^1)^H \boldsymbol{\eta}_{\bar{m},\bar{n}}\}\right)^2\right] & \cdots & 0 \\ \vdots & & \ddots & \vdots \\ 0 & \cdots & & \mathbb{E}\left[\left(\Re\{\left[(\widehat{\mathbf{G}}_{\bar{m}}^H \widehat{\mathbf{G}}_{\bar{m}})^{-1}\right]_{K,K} (\widehat{\mathbf{g}}_{\bar{m}}^K)^H \boldsymbol{\eta}_{\bar{m},\bar{n}}\}\right)^2\right] \end{bmatrix}.\end{aligned} \tag{44}$$

The kth diagonal entry of (44) can be simplified as follows

$$\begin{aligned}&\mathbb{E}\left[\left(\Re\{\left[(\widehat{\mathbf{G}}_{\bar{m}}^H \widehat{\mathbf{G}}_{\bar{m}})^{-1}\right]_{k,k} (\widehat{\mathbf{g}}_{\bar{m}}^k)^H \boldsymbol{\eta}_{\bar{m},\bar{n}}\}\right)^2\right] \\ &= \mathbb{E}\left[\left(\Re\{\left[(\widehat{\mathbf{G}}_{\bar{m}}^H \widehat{\mathbf{G}}_{\bar{m}})^{-1}\right]_{k,k}\}\right)^2 \left(\Re\{(\widehat{\mathbf{g}}_{\bar{m}}^k)^H \boldsymbol{\eta}_{\bar{m},\bar{n}}\}\right)^2\right] \\ &+ \left(\Im\{\left[(\widehat{\mathbf{G}}_{\bar{m}}^H \widehat{\mathbf{G}}_{\bar{m}})^{-1}\right]_{k,k}\}\right)^2 \left(\Im\{(\widehat{\mathbf{g}}_{\bar{m}}^k)^H \boldsymbol{\eta}_{\bar{m},\bar{n}}\}\right)^2\Big].\end{aligned} \tag{45}$$

Using $\mathbb{E}\left[\left(\Re\{(\widehat{\mathbf{g}}_{\bar{m}}^k)^H \boldsymbol{\eta}_{\bar{m},\bar{n}}\}\right)^2\right] = \mathbb{E}\left[\left(\Im\{(\widehat{\mathbf{g}}_{\bar{m}}^k)^H \boldsymbol{\eta}_{\bar{m},\bar{n}}\}\right)^2\right] = \left[(\widehat{\mathbf{G}}_{\bar{m}}^H \widehat{\mathbf{G}}_{\bar{m}})\right]_{k,k} \frac{\sigma_\eta^2}{2}$, (45) can therefore be finally expressed as

$$\begin{aligned}\left[\text{Cov}\left[\Re\{\widehat{\mathbf{G}}_{\bar{m}}^{\dagger} \boldsymbol{\eta}_{\bar{m},\bar{n}}\}\right]\right]_{k,k} &= \mathbb{E}\left[\left(\Re\{\left[(\widehat{\mathbf{G}}_{\bar{m}}^H \widehat{\mathbf{G}}_{\bar{m}})^{-1}\right]_{k,k} (\widehat{\mathbf{g}}_{\bar{m}}^k)^H \boldsymbol{\eta}_{\bar{m},\bar{n}}\}\right)^2\right] \\ &= \left[(\widehat{\mathbf{G}}_{\bar{m}}^H \widehat{\mathbf{G}}_{\bar{m}})^{-1}\right]_{k,k} \frac{\sigma_\eta^2}{2}.\end{aligned} \tag{46}$$

Along similar lines, the first term of (43) is simplified as

$$\begin{aligned}\left[\text{Cov}\left[\Re\{\widehat{\mathbf{G}}_{\bar{m}}^{\dagger} \mathbf{E}_{\bar{m}} \mathbf{b}_{\bar{m},\bar{n}}\}\right]\right]_{k,k} &= \left[(\widehat{\mathbf{G}}_{\bar{m}}^H \widehat{\mathbf{G}}_{\bar{m}})^{-2}\right]_{k,k} \\ &\times (\widehat{\mathbf{g}}_{\bar{m}}^k)^H \left(\sum_{j=1}^{K} P_j \mathbf{e}_{\bar{m}}^j (\mathbf{e}_{\bar{m}}^j)^H\right) \widehat{\mathbf{g}}_{\bar{m}}^k.\end{aligned} \tag{47}$$

Therefore, using (46) and (47), the covariance of $\overline{\boldsymbol{\vartheta}}_{\bar{m},\bar{n}}^{\text{ZF}}$ in (43) can be written as

$$\begin{aligned}&\left[\text{Cov}\left[\boldsymbol{\vartheta}_{\bar{m},\bar{n}}^{\text{ZF}}\right]\right]_{k,k} \\ &= \left[(\widehat{\mathbf{G}}_{\bar{m}}^H \widehat{\mathbf{G}}_{\bar{m}})^{-2}\right]_{k,k} \left((\widehat{\mathbf{g}}_{\bar{m}}^k)^H \left(\sum_{j=1}^{K} P_j \mathbf{e}_{\bar{m}}^j (\mathbf{e}_{\bar{m}}^j)^H\right) \widehat{\mathbf{g}}_{\bar{m}}^k\right) \\ &+ \left[(\widehat{\mathbf{G}}_{\bar{m}}^H \widehat{\mathbf{G}}_{\bar{m}})^{-1}\right]_{k,k} \frac{\sigma_\eta^2}{2}.\end{aligned} \tag{48}$$

APPENDIX C

Similar to Appendix A, the power of the $\overline{\vartheta}_{\bar{m},\bar{n}}^{k,\text{MRC}}$, which forms the denominator of (20), obtained by replacing $\mathbf{w}_{\bar{m}}^k$ with $\widehat{\mathbf{g}}_{\bar{m}}^k$ in (18), can be determined as

$$\begin{aligned}\text{Var}\left[\overline{\vartheta}_{\bar{m},\bar{n}}^{k,\text{MRC}}\right] &= P_k \text{Var}\left[\left(\widehat{\mathbf{g}}_{\bar{m}}^k\right)^H \mathbf{g}_{\bar{m}}^k\right] + \sum_{\substack{j=1\\ j\neq k}}^{K} P_j \mathbb{E}\left[\left|\left(\widehat{\mathbf{g}}_{\bar{m}}^k\right)^H \mathbf{g}_{\bar{m}}^j\right|^2\right] \\ &+ \mathbb{E}\left\{\|\widehat{\mathbf{g}}_{\bar{m}}^k\|^2\right\} \frac{\sigma_\eta^2}{2}.\end{aligned} \tag{49}$$

The terms of $\text{Var}\left[\overline{\vartheta}_{\bar{m},\bar{n}}^{k,\text{MRC}}\right]$ in (49) can be further simplified to derive the closed-form expression of (20).

Exploiting the statistical property that the estimated channel $\widehat{g}_{\bar{m},n}^k \sim \mathcal{CN}\left(0, \frac{P_p(\beta_k)^2}{(P_p\beta_k + {\sigma_\eta}^2)}\right)$, the desired signal power in the numerator of (20) can be further simplified to obtain the closed-form expression as

$$\left|\mathbb{E}\left[\left(\widehat{\mathbf{g}}_{\bar{m}}^k\right)^H \mathbf{g}_{\bar{m}}^k\right]\right|^2 = \left(N \frac{P_p\left(\beta_k\right)^2}{\left(P_p\beta_k + {\sigma_\eta}^2\right)}\right)^2. \tag{50}$$

It is important to note here that the channel estimate $\widehat{\mathbf{g}}_{\bar{m}}^k$ and channel estimation error $\mathbf{e}_{\bar{m}}^k$ are independent of each other. It therefore follows that $\mathbb{E}\left[\left(\widehat{\mathbf{g}}_{\bar{m}}^k\right)^H \mathbf{e}_{\bar{m}}^k\right] = 0$. Consequently, $\mathbb{E}\left[\left(\widehat{\mathbf{g}}_{\bar{m}}^k\right)^H \mathbf{g}_{\bar{m}}^k\right]$ can be computed as $\mathbb{E}\left[\left(\widehat{\mathbf{g}}_{\bar{m}}^k\right)^H \widehat{\mathbf{g}}_{\bar{m}}^k\right]$.

The first term in the denominator of (20) can be further simplified using the joint statistics of $\widehat{\mathbf{g}}_{\bar{m}}^k$ and $\mathbf{g}_{\bar{m}}^k$ as

$$\begin{aligned}\text{Var}\left[\left(\widehat{\mathbf{g}}_{\bar{m}}^k\right)^H \mathbf{g}_{\bar{m}}^k\right] &= \mathbb{E}\left[\left|\left(\widehat{\mathbf{g}}_{\bar{m}}^k\right)^H \mathbf{g}_{\bar{m}}^k\right|^2\right] - \left(\mathbf{E}[\left(\widehat{\mathbf{g}}_{\bar{m}}^k\right)^H \mathbf{g}_{\bar{m}}^k]\right)^2 \\ &\overset{(a)}{=} \mathbb{E}\left[\left|\left(\widehat{\mathbf{g}}_{\bar{m}}^k\right)^H \widehat{\mathbf{g}}_{\bar{m}}^k\right|^2\right] + \mathbb{E}\left[\left|\left(\widehat{\mathbf{g}}_{\bar{m}}^k\right)^H \mathbf{e}_{\bar{m}}^k\right|^2\right] \\ &- \left(\mathbf{E}[\left(\widehat{\mathbf{g}}_{\bar{m}}^k\right)^H \mathbf{g}_{\bar{m}}^k]\right)^2 \\ &\overset{(b)}{=} \mathbb{E}\left[\sum_{i=1}^{N} \left|\widehat{g}_{\bar{m},i}^k\right|^4 + 2\sum_{\substack{i=1\\ j>i}}^{\binom{N}{2}} \left(\left|\widehat{g}_{\bar{m},i}^k\right|^2 \left|\widehat{g}_{\bar{m},j}^k\right|^2\right)\right] \\ &+ \mathbb{E}\left[\left|\left(\widehat{\mathbf{g}}_{\bar{m}}^k\right)^H \mathbf{e}_{\bar{m}}^k\right|^2\right] - \left(\mathbf{E}[\left(\widehat{\mathbf{g}}_{\bar{m}}^k\right)^H \mathbf{g}_{\bar{m}}^k]\right)^2.\end{aligned} \tag{51}$$

The equality (a) is obtained by using the relationship $\mathbf{g}_{\bar{m}}^k = \widehat{\mathbf{g}}_{\bar{m}}^k + \mathbf{e}_{\bar{m}}^k$, whereas equality (b) is obtained by further simplifying the first term of equality (a). Exploiting the statistical properties of the estimated channel and using $\mathbb{E}\left[\left|\widehat{g}_{\bar{m},n}^k\right|^4\right] = 2\left(\mathbb{E}\left[\left(\widehat{g}_{\bar{m},n}^k\right)^2\right]\right)^2 = 2\left(\frac{P_p(\beta_k)^2}{(P_p\beta_k + {\sigma_\eta}^2)}\right)^2$, the above expression can be simplified as

$$\begin{aligned}\text{Var}\left[\left(\widehat{\mathbf{g}}_{\bar{m}}^k\right)^H \mathbf{g}_{\bar{m}}^k\right] &= 2N\left(\frac{P_p\left(\beta_k\right)^2}{\left(P_p\beta_k + \sigma_\eta^2\right)}\right)^2 + N(N-1)\left(\frac{P_p\left(\beta_k\right)^2}{\left(P_p\beta_k + \sigma_\eta^2\right)}\right)^2 \\ &+ \frac{NP_p\left(\beta_k\right)^3 \sigma_\eta^2}{\left(P_p\beta_k + \sigma_\eta^2\right)^2} - \left(\frac{NP_p\left(\beta_k\right)^2}{\left(P_p\beta_k + \sigma_\eta^2\right)}\right)^2.\end{aligned} \tag{52}$$

Simplifying this yields the closed-form expression of $\text{Var}\left[\left(\widehat{\mathbf{g}}_{\bar{m}}^k\right)^H \mathbf{g}_{\bar{m}}^k\right]$ given as

$$\text{Var}\left[\left(\widehat{\mathbf{g}}_{\bar{m}}^k\right)^H \mathbf{g}_{\bar{m}}^k\right] = \frac{N\left(P_p\left(\beta_k\right)^2\right)^2 + NP_p\left(\beta_k\right)^3 \sigma_\eta^2}{\left(\left(P_p\beta_k + \sigma_\eta^2\right)\right)^2}. \tag{53}$$

Along similar lines, the power of the inter-user interference $\mathbb{E}\left[\left|\left(\widehat{\mathbf{g}}_{\bar{m}}^k\right)^H \mathbf{g}_{\bar{m}}^j\right|^2\right]$ can be simplified by using the joint statistics of $\widehat{\mathbf{g}}_{\bar{m}}^k$ and $\mathbf{g}_{\bar{m}}^j$ formulated as

$$\sum_{\substack{j=1\\ j\neq k}}^{K}\mathbb{E}\big[\big|\big(\widehat{\mathbf{g}}_{\bar{m}}^{k}\big)^{H}\mathbf{g}_{\bar{m}}^{j}\big|^{2}\big]=\sum_{\substack{j=1\\ j\neq k}}^{K}\frac{N\left(P_p\right)^2(\beta_k\beta_j)^2+NP_p(\beta_k)^2\beta_j\sigma_\eta^2}{\left(P_p\beta_k+{\sigma_\eta}^2\right)\left(P_p\beta_j+{\sigma_\eta}^2\right)}. \tag{54}$$

The last term in the denominator of (20) is the power of the resultant noise after applying the combiner at the BS and can be simplified by exploiting the property that the noise added at the BS is statistically independent of the combiner. Using the statistical properties of the estimated channel in Section II-B, the power of the resultant noise can be simplified as

$$\mathbb{E}\big\{\|\widehat{\mathbf{g}}_{\bar{m}}^{k}\|^2\big\}\frac{\sigma_\eta^2}{2}=N\frac{P_p\left(\beta_k\right)^2}{\left(P_p\beta_k+{\sigma_\eta}^2\right)}\times\frac{\sigma_\eta^2}{2}. \tag{55}$$

APPENDIX D

Using $\mathbf{W}_{\bar{m}}=(\widehat{\mathbf{G}}_{\bar{m}}^{\dagger})^{H}=\widehat{\mathbf{G}}_{\bar{m}}(\widehat{\mathbf{G}}_{\bar{m}}^{H}\widehat{\mathbf{G}}_{\bar{m}})^{-1}$ in (17), the received signal can be simplified as follows

$$\begin{aligned}\widehat{\mathbf{G}}_{\bar{m}}^{\dagger}\mathbf{y}_{\bar{m},\bar{n}}=&\mathbb{E}\big[\widehat{\mathbf{G}}_{\bar{m}}^{\dagger}\mathbf{G}_{\bar{m}}\big]\mathbf{b}_{\bar{m},\bar{n}}\\&+\big(\widehat{\mathbf{G}}_{\bar{m}}^{\dagger}\mathbf{G}_{\bar{m}}-\mathbb{E}\big[\widehat{\mathbf{G}}_{\bar{m}}^{\dagger}\mathbf{G}_{\bar{m}}\big]\big)\mathbf{b}_{\bar{m},\bar{n}}+\widehat{\mathbf{G}}_{\bar{m}}^{\dagger}\boldsymbol{\eta}_{\bar{m},\bar{n}}.\end{aligned} \tag{56}$$

The estimate of the OQAM transmitted signal, in terms of the desired signal and the effective noise components over the index $(\bar{m},\bar{n})$, can be written as

$$\widehat{\mathbf{d}}_{\bar{m},\bar{n}}=\Re\big\{\widehat{\mathbf{G}}_{\bar{m}}^{\dagger}\mathbf{y}_{\bar{m},\bar{n}}\big\}=\underbrace{\Re\big\{\mathbf{b}_{\bar{m},\bar{n}}\big\}}_{\text{Desired Signal}}+\underbrace{\overline{\boldsymbol{\vartheta}}_{\bar{m},\bar{n}}^{\text{ZF}}}_{\text{Effective Noise}}, \tag{57}$$

where the term $\overline{\boldsymbol{\vartheta}}_{\bar{m},\bar{n}}^{\text{ZF}}$ is expressed as

$$\overline{\boldsymbol{\vartheta}}_{\bar{m},\bar{n}}^{\text{ZF}}=\underbrace{\Re\big\{\big(\widehat{\mathbf{G}}_{\bar{m}}^{\dagger}\mathbf{G}_{\bar{m}}-\mathbb{E}\big[\widehat{\mathbf{G}}_{\bar{m}}^{\dagger}\mathbf{G}_{\bar{m}}\big]\big)\mathbf{b}_{\bar{m},\bar{n}}\big\}}_{\text{Beamforming Uncertainty}}+\underbrace{\Re\big\{\widehat{\mathbf{G}}_{\bar{m}}^{\dagger}\boldsymbol{\eta}_{\bar{m},\bar{n}}\big\}}_{\text{Noise}}. \tag{58}$$

Using $\mathbf{G}_{\bar{m}}=\widehat{\mathbf{G}}_{\bar{m}}+\mathbf{E}_{\bar{m}}$, the term $\overline{\boldsymbol{\vartheta}}_{\bar{m},\bar{n}}^{\text{ZF}}$ in (58) can be further simplified as $\overline{\boldsymbol{\vartheta}}_{\bar{m},\bar{n}}^{\text{ZF}}=\Re\big\{\big(\widehat{\mathbf{G}}_{\bar{m}}^{\dagger}\mathbf{E}_{\bar{m}}-\mathbb{E}\big[\widehat{\mathbf{G}}_{\bar{m}}^{\dagger}\mathbf{E}_{\bar{m}}\big]\big)\mathbf{b}_{\bar{m},\bar{n}}\big\}+\Re\big\{\widehat{\mathbf{G}}_{\bar{m}}^{\dagger}\boldsymbol{\eta}_{\bar{m},\bar{n}}\big\}$. Therefore, the covariance matrix of the effective noise can be expressed as

$$\begin{aligned}\text{Cov}\big[\overline{\boldsymbol{\vartheta}}_{\bar{m},\bar{n}}^{\text{ZF}}\big]=&\mathbb{E}\big[\overline{\boldsymbol{\vartheta}}_{\bar{m},\bar{n}}^{\text{ZF}}(\overline{\boldsymbol{\vartheta}}_{\bar{m},\bar{n}}^{\text{ZF}})^{H}\big]\\=&\text{Cov}\big[\Re\{\widehat{\mathbf{G}}_{\bar{m}}^{\dagger}\mathbf{E}_{\bar{m}}\mathbf{b}_{\bar{m},\bar{n}}\}\big]+\text{Cov}\big[\Re\{\widehat{\mathbf{G}}_{\bar{m}}^{\dagger}\boldsymbol{\eta}_{\bar{m},\bar{n}}\}\big].\end{aligned} \tag{59}$$

The simplified expression of the power of $\Big[\text{Cov}\big[\overline{\boldsymbol{\vartheta}}_{\bar{m},\bar{n}}^{\text{ZF}}\big]\Big]_{k,k}$, which forms the denominator of (23), is given by

$$\begin{aligned}\Big[\text{Cov}\big[\overline{\boldsymbol{\vartheta}}_{\bar{m},\bar{n}}^{\text{ZF}}\big]\Big]_{k,k}=&\Big(\sum_{j=1}^{K}P_j\mathbb{E}\big[e_{\bar{m}}^{j}(e_{\bar{m}}^{j})^{*}\big]+\frac{\sigma_\eta^2}{2}\Big)\\&\times\mathbb{E}\big[\big\{(\widehat{\mathbf{G}}_{\bar{m}}^{H}\widehat{\mathbf{G}}_{\bar{m}})^{-1}\big\}_{k,k}\big],\end{aligned} \tag{60}$$

where we have $\mathbb{E}\big[e_{\bar{m}}^{j}(e_{\bar{m}}^{j})^{*}\big]=\mathbb{E}\big[\{\mathbf{e}_{\bar{m}}^{j}(\mathbf{e}_{\bar{m}}^{j})^{H}\}_{i,i}\big]$, for $i=1,,2,\cdots,N$.

The denominator of $\overline{\text{SINR}}_{\bar{m},k}^{\text{ZF}}$ in (23) contains quantities that can be further simplified by using the channel estimation error statistics and the identity $\mathbb{E}\big[\text{Tr}(\mathbf{W}^{-1})\big]=\frac{l}{n-l}$ [56], where $\mathbf{W}\in\mathbb{C}^{n\times n}$ is a central complex Wishart matrix with n $(n>l)$ degrees of freedom. Therefore, substituting $\mathbb{E}\big[\big\{(\widehat{\mathbf{G}}_{\bar{m}}^{H}\widehat{\mathbf{G}}_{\bar{m}})^{-1}\big\}_{k,k}\big]=\frac{P_p\beta_k+1}{(N-K)P_p\beta_k^2}$, the terms of the quantity $\overline{\text{SINR}}_{\bar{m},k}^{\text{ZF}}$ in (23) are simplified to obtain the closed-from expression.

APPENDIX E

The problem **P4** can be seen as an outer optimization over the power variables P_k and an inner optimization over $t_{\bar{m},k}^{\Delta}$ for a fixed P_k. It follows from (30a) that the inner optimization problem can be solved by satisfying the constraint (30b) with equality as

$$t_{\bar{m},k}^{\Delta\ *}=\frac{\text{N}_{\bar{m},k}^{\Delta}(\mathbf{p})}{\text{D}_{\bar{m},k}^{\Delta}(\mathbf{p})}. \tag{61}$$

The corresponding Lagrangian function associated with the inner optimization problem in **P4** can be written as

$$\mathcal{L}\big(t_{\bar{m},k}^{\Delta},\lambda_{\bar{m},k}^{\Delta}\big)=\frac{\big(\frac{\tau_d}{T}\big)\sum_{k=1}^{K}\log_2\big(1+t_{\bar{m},k}^{\Delta}\big)}{\mathcal{P}_{\text{tot}}(\mathbf{p})}-\sum_{k=1}^{K}\lambda_{\bar{m},k}^{\Delta}\Big(t_{\bar{m},k}^{\Delta}-\frac{\text{N}_{\bar{m},k}^{\Delta}(\mathbf{p})}{\text{D}_{\bar{m},k}^{\Delta}(\mathbf{p})}\Big), \tag{62}$$

where $\Big\{\lambda_{\bar{m},1}^{\Delta},\lambda_{\bar{m},2}^{\Delta}\cdots,\lambda_{\bar{m},k}^{\Delta}\Big\}$ are the Lagrangian multipliers associated with the inequality constraints in (30b). The problem **P4** is convex and Slater's condition holds. Therefore, strong duality exists for (62). The dual of the optimization problem in (62) can be written as $\underset{\lambda_{\bar{m},k}^{\Delta}}{\text{Min}}\ \underset{t_{\bar{m},k}^{\Delta}}{\text{Max}}\ \mathcal{L}\big(t_{\bar{m},k}^{\Delta},\lambda_{\bar{m},k}^{\Delta}\big)$. Let $\big\{t_{\bar{m},k}^{\Delta\ *},\lambda_{\bar{m},k}^{\Delta\ *}\big\}$ denote the saddle point of the above problem. Therefore, the optimal $\lambda_{\bar{m},k}^{\Delta\ *}$ can be calculated by setting $\frac{\partial\mathcal{L}\left(t_{\bar{m},k}^{\Delta},\lambda_{\bar{m},k}^{\Delta}\right)}{\partial t_{\bar{m},k}^{\Delta}}=0$ as

$$\lambda_{\bar{m},k}^{\Delta\ *}=\frac{1}{\log_e(2)\mathcal{P}_{\text{tot}}(\mathbf{p})\big(1+t_{\bar{m},k}^{\Delta\ *}\big)}. \tag{63}$$

Substituting $\lambda_{\bar{m},k}^{\Delta\ *}$ and $t_{\bar{m},k}^{\Delta\ *}$ in (62) and (63), $\mathcal{L}\big(P_k,t_{\bar{m},k}^{\Delta},\lambda_{\bar{m},k}^{\Delta\ *}\big)$ can be expressed as

$$\mathcal{L}\big(t_{\bar{m},k}^{\Delta},\lambda_{\bar{m},k}^{\Delta\ *}\big)=\frac{\left\{\begin{array}{l}\Big(\frac{\tau_d}{T}\Big)\sum_{k=1}^{K}\log_2\left(1+t_{\bar{m},k}^{\Delta}\right)\\-\frac{1}{\log_e(2)}\sum_{k=1}^{K}\frac{\text{D}_{\bar{m},k}^{\Delta}(\mathbf{p})}{t_{\bar{m},k}^{\Delta}}-\frac{\text{N}_{\bar{m},k}^{\Delta}(\mathbf{p})}{t_{\bar{m},k}^{\Delta}}\end{array}\right\}}{\mathcal{P}_{\text{tot}}(\mathbf{p})}. \tag{64}$$

After some mathematical manipulations and combining with the outer maximization over P_k in **P4**, the above expression is simplified to $f_{\mathcal{L}}\big(\mathbf{p},\mathbf{t}_{\bar{m}}^{\Delta}\big)$ as given in **P5**.

REFERENCES

[1] X. You *et al.*, "Towards 6G wireless communication networks: vision, enabling technologies, and new paradigm shifts," *Sci. China Inf. Sci.*, vol. 64, no. 1, p. 110301, Nov 2020. [Online]. Available: https://doi.org/10.1007/s11432-020-2955-6

[2] B. Farhang-Boroujeny, "OFDM versus filter bank multicarrier," *IEEE Signal Process. Mag.*, vol. 28, no. 3, pp. 92–112, 2011.

[3] R. Nissel, S. Schwarz, and M. Rupp, "Filter bank multicarrier modulation schemes for future mobile communications," *IEEE J. Select. Areas Commun.*, vol. 35, no. 8, pp. 1768–1782, 2017.

[4] B. Farhang-Boroujeny and H. Moradi, "OFDM inspired waveforms for 5G," *IEEE Commun. Surveys Tuts*, vol. 18, no. 4, pp. 2474–2492, 2016.

[5] K.-C. Lai *et al.*, "A family of MMSE-based decision feedback equalizers and their properties for FBMC/OQAM systems," *IEEE Trans. Veh. Technol.*, vol. 68, no. 3, pp. 2346–2360, 2019.

[6] D. Chen *et al.*, "Low-complexity symbol reconstruction based on direct symbol decision for FBMC-OQAM systems," *IEEE Trans. Signal Process*, vol. 71, pp. 4369–4381, 2023.

[7] P. Singh *et al.*, "Semi-blind, training, and data-aided channel estimation schemes for MIMO-FBMC-OQAM systems," *IEEE Trans. Signal Process.*, vol. 67, no. 18, pp. 4668–4682, 2019.

[8] E. Kofidis *et al.*, "Preamble-based channel estimation in OFDM/OQAM systems: A review," *Signal Process.*, vol. 93, no. 7, pp. 2038–2054, 2013.

[9] R. Nissel and M. Rupp, "Enabling low-complexity MIMO in FBMC-OQAM," in *2016 IEEE Globecom Workshops (GC Wkshps)*, 2016, pp. 1–6.

[10] R. Nissel, J. Blumenstein, and M. Rupp, "Block frequency spreading: A method for low-complexity MIMO in FBMC-OQAM," in *2017 IEEE 18th International Workshop on Signal Processing Advances in Wireless Communications (SPAWC)*, 2017, pp. 1–5.

[11] R. Zakaria and D. Le Ruyet, "A novel filter-bank multicarrier scheme to mitigate the intrinsic interference: Application to MIMO systems," *IEEE Trans. Wireless Commun.*, vol. 11, no. 3, pp. 1112–1123, 2012.

[12] Y. Xu *et al.*, "An imaginary interference-free method for MIMO precoding in FBMC/OQAM systems," *IEEE Trans. Broadcast.*, vol. 67, no. 3, pp. 642–650, 2021.

[13] A. Farhang *et al.*, "Filter bank multicarrier for massive MIMO," in *Proc. IEEE 80th Veh. Technol. Conf. VTC Fall*, 2014, pp. 1–7.

[14] F. Rottenberg *et al.*, "Performance analysis of linear receivers for uplink massive MIMO FBMC-OQAM systems," *IEEE Trans. Signal Process*, vol. 66, no. 3, pp. 830–842, 2018.

[15] A. Aminjavaheri, A. Farhang, and B. Farhang-Boroujeny, "Filter bank multicarrier in massive MIMO: Analysis and channel equalization," *IEEE Trans. Signal Process*, vol. 66, no. 15, pp. 3987–4000, 2018.

[16] A. Aminjavaheri *et al.*, "Prototype filter design for FBMC in massive MIMO channels," in *Proc. IEEE Int. Conf. Commun. (ICC)*, 2017, pp. 1–6.

[17] H. Hosseiny, A. Farhang, and B. Farhang-Boroujeny, "FBMC receiver design and analysis for medium and large scale antenna systems," *IEEE Trans. Veh. Technol.*, vol. 71, no. 3, pp. 3044–3057, 2022.

[18] P. Singh *et al.*, "Uplink sum-rate and power scaling laws for multi-user massive MIMO-FBMC systems," *IEEE Trans. Commun. Technol.*, vol. 68, no. 1, pp. 161–176, 2020.

[19] S. Singh *et al.*, "Uplink transmission in MU multi-cell massive MIMO-FBMC systems over ricean fading," in *Proc. IEEE 94th Veh. Technol. Conf. VTC Fall*, 2021, pp. 01–06.

[20] F. Hamdar *et al.*, "Overlap-save FBMC receivers for massive MIMO systems under channel impairments," in *Proc. IEEE 95th Veh. Technol. Conf. VTC Spring*, 2022, pp. 1–7.

[21] Y. Qi *et al.*, "Efficient channel equalization and performance analysis for uplink FBMC/OQAM-based massive MIMO systems," *IEEE Trans. Veh. Technol.*, vol. 72, no. 9, pp. 11 532–11 547, 2023.

[22] M. Masarra *et al.*, "FBMC-OQAM for frequency-selective mmwave hybrid MIMO systems," in *IEEE Wireless Commun. Netw. Conf. WCNC*, 2022, pp. 1593–1598.

[23] D. Kong *et al.*, "Frame repetition: A solution to imaginary interference cancellation in FBMC/OQAM systems," *IEEE Trans. Signal Process*, vol. 68, pp. 1259–1273, 2020.

[24] D. Sim *et al.*, "A signal-level maximum likelihood detection based on partial candidates for MIMO FBMC-QAM system with two prototype filters," *IEEE Trans. Veh. Technol.*, vol. 68, no. 3, pp. 2598–2608, 2019.

[25] L.-H. Shen, K.-T. Feng, and L. Hanzo, "Five facets of 6G: Research challenges and opportunities," *ACM Comput. Surv.*, vol. 55, no. 11, pp. 1–39, 2023.

[26] D. Ying, D. J. Love, and B. M. Hochwald, "Closed-loop precoding and capacity analysis for multiple-antenna wireless systems with user radiation exposure constraints," *IEEE Trans. Wireless Commun.*, vol. 14, no. 10, pp. 5859–5870, 2015.

[27] C.-X. Wang *et al.*, "On the road to 6G: Visions, requirements, key technologies and testbeds," *IEEE Commun. Surv. Tutor.*, pp. 1–1, 2023.

[28] M. A. Jamshed *et al.*, "Emission-aware resource optimization framework for backscatter-enabled uplink NOMA networks," in *Proc. IEEE 95th Veh. Technol. Conf. VTC Spring*, 2022, pp. 1–5.

[29] R. Cleveland, "Compliance with FCC exposure guidelines for radiofrequency electromagnetic fields," in *IEEE Int. Symp. Electromagn. Compat. (IEEE Cat. No.04CH37559)*, vol. 3, 2004, pp. 1030–1035 vol.3.

[30] M. Tesanovic *et al.*, "The LEXNET project: Wireless networks and EMF: Paving the way for low-EMF networks of the future," *IEEE Veh. Technol. Mag.*, vol. 9, no. 2, pp. 20–28, 2014.

[31] "ICNIRP guidelines on limiting exposure to time-varying electric, magnetic and electromagnetic fields (100 kHz to 300 GHz)."

[32] J. Denis, M. Pischella, and D. Le Ruyet, "Energy-efficiency-based resource allocation framework for cognitive radio networks with FBMC/OFDM," *IEEE Trans. Veh. Technol.*, vol. 66, no. 6, pp. 4997–5013, 2017.

[33] J. Xiong *et al.*, "Energy-efficient precoding in electromagnetic exposure-constrained uplink multiuser MIMO," *IEEE Trans. Veh. Technol.*, vol. 70, no. 7, pp. 7226–7231, 2021.

[34] H. Jiang *et al.*, "Multiuser MIMO uplink transmission with electromagnetic exposure constraints: Spectral efficiency and energy efficiency tradeoff," *IEEE Commun. Lett.*

[35] Z. Lou, A. Elzanaty, and M.-S. Alouini, "Green tethered UAVs for EMF-aware cellular networks," *IEEE Trans. Green Commun. Netw.*, vol. 5, no. 4, pp. 1697–1711, 2021.

[36] M. A. Jamshed, F. Héliot, and T. W. C. Brown, "Unsupervised learning based emission-aware uplink resource allocation scheme for non-orthogonal multiple access systems," *IEEE Trans. Veh. Technol.*, vol. 70, no. 8, pp. 7681–7691, 2021.

[37] H. Jiang *et al.*, "Hybrid RIS and DMA assisted multiuser MIMO uplink transmission with electromagnetic exposure constraints," *IEEE J. Sel. Topics Signal Process.*, vol. 16, no. 5, pp. 1055–1069, 2022.

[38] F. Héliot and T. W. C. Brown, "On the exposure dose minimization of multi-antenna multi-carrier system users," *IEEE Trans. Veh. Technol.*, vol. 71, no. 7, pp. 7625–7638, 2022.

[39] A. Zappone and M. D. Renzo, "Energy efficiency optimization of reconfigurable intelligent surfaces with electromagnetic field exposure constraints," *IEEE Signal Process. Lett.*, vol. 29, pp. 1447–1451, 2022.

[40] H. Ibraiwish *et al.*, "EMF-aware cellular networks in RIS-assisted environments," *IEEE Commun. Lett.*, vol. 26, no. 1, pp. 123–127, 2022.

[41] S. Aghashahi *et al.*, "EMF-aware energy efficient MU-SIMO systems with multiple RISs," *IEEE Trans. Veh. Technol.*, vol. 73, no. 5, pp. 7339–7344, 2024.

[42] Y. A. Sambo *et al.*, "Electromagnetic emission-aware resource allocation

for the uplink of OFDM wireless communication systems," in *2015 International Symposium on Wireless Communication Systems (ISWCS)*, 2015, pp. 441–445.

[43] V. Mandawaria, E. Sharma, and R. Budhiraja, "Energy-efficient massive MIMO multi-relay NOMA systems with CSI errors," *IEEE Trans. Commun.*, vol. 68, no. 12, pp. 7410–7428, 2020.

[44] E. Björnson *et al.*, "Massive MIMO networks: Spectral, energy, and hardware efficiency," *Foundations and Trends® in Signal Processing*, vol. 11, no. 3-4, pp. 154–655, 2017.

[45] A. Bazin, B. Jahan, and M. Hélard, "Impact of the doppler effect on the capacity of massive MIMO uplink systems: OFDM versus FBMC/OQAM," in *Proc. 24th Int. Conf. Telecommun. ICT*, 2017, pp. 1–6.

[46] S. Mahama *et al.*, "Multi-user wireless information and power transfer in FBMC-based IoT networks," *IEEE open j. Commun. Soc.*, vol. 2, pp. 545–563, 2021.

[47] J. C. Estrada-Jiménez *et al.*, "Power allocation and capacity analysis for FBMC-OQAM with superimposed training," *IEEE Access*, vol. 7, pp. 46 968–46 976, 2019.

[48] M. Kobayashi, N. Jindal, and G. Caire, "Training and feedback optimization for multiuser MIMO downlink," *IEEE Trans. Commun.*, vol. 59, no. 8, pp. 2228–2240, 2011.

[49] H. Wang *et al.*, "Preamble design with interference cancellation for channel estimation in MIMO-FBMC/OQAM systems," *IEEE Access*, vol. 6, pp. 44 072–44 081, 2018.

[50] S. M. Kay, *Fundamentals of statistical signal processing: estimation theory*. Prentice-Hall, Inc., 1993.

[51] K. Shen and W. Yu, "Fractional programming for communication systems—part I: Power control and beamforming," *IEEE Trans. Signal Process.*, vol. 66, no. 10, pp. 2616–2630, 2018.

[52] M. Grant and S. Boyd, "CVX: matlab software for disciplined convex programming, version 2.1," http://cvxr.com/cvx, Mar. 2014.

[53] K. Shen and W. Yu, "Fractional programming for communication systems—part II: Uplink scheduling via matching," *IEEE Trans. Signal Process.*, vol. 66, no. 10, pp. 2631–2644, 2018.

[54] W. Dinkelbach, "On nonlinear fractional programming," *Management science*, vol. 13, no. 7, pp. 492–498, 1967.

[55] S. Dey, E. Sharma, and R. Budhiraja, "Hardware-impaired rician-faded massive MIMO FD relay: Analysis and optimization," *IEEE Trans. Commun. Technol.*, vol. 69, no. 8, pp. 5209–5227, 2021.

[56] A. M. Tulino, S. Verdú *et al.*, "Random matrix theory and wireless communications," *Foundations and Trends® in Communications and Information Theory*, vol. 1, no. 1, pp. 1–182, 2004.